Gut Microbe-Derived Trimethylamine Shapes Circadian Rhythms Through the Host Receptor TAAR5.

Kala K. Mahen[1-3], William J. Massey[2,4], Danny Orabi[1], Amanda L. Brown[1], Thomas C. Jaramillo[5], Amy C. Burrows[1], Anthony J. Horak III[1], Sumita Dutta[1,2], Marko Mrdjen[1-4], Nour Mouannes[1-3], Venkateshwari Varadharajan[1,2], Lucas J. Osborn[1-3], Xiayan Ye[1], Dante M. Yarbrough[1], Treg Grubb[1], Natalie Zajczenko[1], Rachel Hohe[1-3], Rakhee Banerjee[1], Pranavi Linga[1], Dev Laungani[1], Adeline M. Hajjar[2,7], Naseer Sangwan[2,6], Mohammed Dwidar[2,7], Jennifer A. Buffa[2,7], Garth R. Swanson[8], Zeneng Wang[2,7], and J. Mark Brown[1-3*]

[1]Department of Cancer Biology, Cleveland Clinic, Cleveland, OH 44195, USA
[2]Center for Microbiome and Human Health, Cleveland Clinic; Cleveland, OH, USA.
[3]Department of Molecular Medicine, Cleveland Clinic Lerner College of Medicine of Case Western Reserve University; Cleveland, Ohio, USA.
[4]Department of Inflammation and Immunity, Cleveland Clinic, Cleveland, OH 44195, USA
[5]Rodent Behavior Core, Cleveland Clinic, Cleveland, Ohio, USA
[6]Microbial Sequencing & Analytics Core Facility, Cleveland Clinic, Cleveland, OH 44195, USA
[7]Department of Cardiovascular and Metabolic Sciences, Cleveland Clinic, Cleveland, OH 44195, USA
[8]Department of Medicine, Medical University of South Carolina, Charleston, SC 29425, USA
[*]To whom correspondence should be addressed: Department of Cancer Biology, Cleveland Clinic, Cleveland, OH 44195, USA
Tel: 216-444-8340; Fax: 216-444-9404; E-mail: brownm5@ccf.org

Running Title: TMA and TAAR5 Signaling Impacts Host Circadian Rhythms

Keywords: Microbiome, Circadian, Metabolism, Olfaction

Abstract

Elevated levels of the gut microbe-derived metabolite trimethylamine N-oxide (TMAO) are associated with cardiometabolic disease risk. However, the mechanism(s) linking TMAO production to human disease are incompletely understood. Initiation of the metaorganismal TMAO pathway begins when dietary choline and related metabolites are converted to trimethylamine (TMA) by gut bacteria. Gut microbe-derived TMA can then be further oxidized by host flavin-containing monooxygenases to generate TMAO. Previously, we showed that drugs lowering both TMA and TMAO protect mice against obesity via rewiring of host circadian rhythms. Although most mechanistic studies in the literature have focused on the metabolic end product TMAO, here we have instead tested whether the primary metabolite TMA alters host metabolic homeostasis and circadian rhythms via trace amine-associated receptor 5 (TAAR5). Remarkably, mice lacking the host TMA receptor (*Taar5*$^{-/-}$) have altered circadian rhythms in gene expression, metabolic hormones, gut microbiome composition, and diverse behaviors. Also, mice genetically lacking bacterial TMA production or host TMA oxidation have altered circadian rhythms. These results provide new insights into diet-microbe-host interactions relevant to cardiometabolic disease, and implicate gut bacterial production of TMA and the host receptor that senses TMA (TAAR5) in the physiologic regulation of circadian rhythms in mice.

Introduction

Modern investigation into human disease relies heavily on genetic and genomic approaches, and most assume that human disease is primarily driven by variation in the human genome. However, in the post genomic era we now understand that human genetic variation explains only a small proportion of risk for complex diseases such as obesity, diabetes, and cardiovascular disease (CVD). Instead, in many cases environmental factors are the predominant drivers of cardiometabolic disease pathogenesis. Among all contributing environmental factors, it is clear that dietary patterns, and diet-driven alterations in the gut microbiome, can profoundly impact many common human diseases.[1-4] There are now many examples of diet-microbe-host interactions shaping human disease, but one of the more compelling is the reproducible link between elevated trimethylamine N-oxide (TMAO) levels and cardiovascular disease (CVD) risk.[5-12] TMAO is generated by a metaorganismal (*i.e.* microbe & host) pathway where dietary substrates such as choline, *L*-carnitine, and γ-butyrobetaine are metabolized by gut microbial enzymes to generate the primary metabolite trimethylamine (TMA).[5-12] TMA is then further metabolized by the host enzyme flavin-containing monooxygenase 3 (FMO3) in the liver to produce trimethylamine-N-oxide (TMAO).[10] Elevated TMAO levels are associated with many human diseases including diverse forms of CVD[5-12], obesity[13,14], type 2 diabetes[15,16], chronic kidney disease (CKD)[17,18], neurodegenerative conditions including Parkinson's and Alzheimer's disease[19,20], and several cancers[21,22]. Many of these disease associations have been validated in several large population meta-analyses[23-25] and Mendelian randomization studies[26,27]. The emerging body of evidence supports the notion that elevated TMAO levels are causally related to cardiometabolic disease pathogenesis. In further support, therapies aimed at lowering circulating TMAO levels provide striking protection against cardiometabolic disease in animal models[28-36]. Several independent studies have now shown that inhibition of either the host TMAO-producing enzyme FMO3 or the microbial TMA-

producing enzyme CutC protects against diet-induced atherosclerosis[15,30], heart failure[32], thrombosis[29,31], obesity[13,33], liver disease[34], insulin resistance[13,33], CKD[35,36], and abdominal aortic aneurysm[37].

Even though TMAO lowering therapies are very effective in preclinical animal models, the underlying mechanism(s) linking the metaorganismal production of TMAO to cardiometabolic disease pathogenesis are still incompletely understood. Mechanistic understanding has been hampered by the fact that it is hard to disentangle the pleiotropic effects of dietary substrates (choline, carnitine, γ-butyrobetaine, trimethyllysine, etc.), bacterial production of TMA, and host-driven conversion of TMA to TMAO. At this point, the vast majority of studies have focused on the end product of this pathway TMAO, but it is equally plausible that the primary metabolite TMA may play some role in microbe-host crosstalk related to human disease. There is some evidence that TMAO can promote inflammatory processes via activation of the nucleotide-binding domain, leucine-rich-containing family, pyrin domain-containing-3 (NLRP3) inflammasome and nuclear factor κB (NFκB).[38-41] TMAO can also activate the endoplasmic reticulum (ER) stress kinase PERK (EIF2AK3) in hepatocytes to promote metabolic disturbance.[28] In parallel, TMAO promotes stimulus-dependent calcium release in platelets to promote thrombosis.[8] Although the end product of the pathway TMAO clearly impacts cell signaling in the host to impact cardiometabolic disease, these TMAO-driven mechanisms do not fully explain how elevated TMAO levels contribute to so many diverse diseases in humans. In addition to TMAO-driven signaling mechanisms, we recently reported that major components of the TMAO pathway (choline, TMA, FMO3, and TAAR5) oscillate in a highly circadian fashion.[33] Furthermore, gut microbe-targeted drugs that selectively block TMA production alter host circadian rhythms in the gut microbiome and host phospholipid metabolism.[33] It is important to note that disruption of the circadian clock is a common hallmark of almost all diseases where TMAO levels are elevated[42-45]. To follow up on the potential links between the TMAO pathway

and host circadian disruption here we have used genetic knockout approaches at the level of host sensing of TMA (i.e. *Taar5*$^{-/-}$), gut microbial TMA production (i.e. *cutC*-null microbial communities), and host TMA oxidation (i.e. *Fmo3*$^{-/-}$). Results here further bolster the concept that TMA production and associated TAAR5 activation shapes host circadian rhythms.

Results

Mice Lacking the TMA Receptor TAAR5 Have Altered Circadian Rhythms in Metabolic Homeostasis and Innate Olfactory-Related Behaviors

We recently demonstrated that drugs blocking gut microbial TMA production protect against obesity via rewiring circadian rhythms in the gut microbiome, liver, white adipose tissue and skeletal muscle.[33] Furthermore, we also showed that blocking bacterial TMA production elicited unexpected alterations in olfactory perception of diverse odorant stimuli.[46] Therefore, we have followed up here to further interrogate circadian rhythms in the gut microbiome, liver, white adipose tissue (WAT), skeletal muscle, and olfactory bulb in mice lacking the only known host G protein-coupled receptor (GPCR) that senses TMA known as TAAR5.[47,48] In agreement with our previous report showing that *Taar5* mRNA is expressed in a circadian manner in skeletal muscle[33], *LacZ* reporter expression oscillates with peak expression in the dark cycle in skeletal muscle (Figure 1A). However, unlike the striking impact that choline TMA lyase inhibitors have on the core circadian clock machinery in skeletal muscle[33], mice lacking the TMA receptor (*Taar5*$^{-/-}$)also have largely unaltered circadian gene expression in skeletal muscle, with only nuclear receptor subfamily 1 group D member 1 (*Nr1d1, Rev-Erb*α) showing a modest yet significant delay in acrophase (Figure 1A; Table 1). Instead, *Taar5*$^{-/-}$ mice have alterations in the expression of key circadian genes including basic helix-loop-helix ARNT like 1 (*Arntl;Bmal*), clock circadian regulator (*Clock*), *Nr1d1, Rev-Erb*α, cryptochrome 1 (*Cry1*), and period 2 (*Per2*) in the olfactory bulb (Figure

1B; Table 1). *Taar5*$^{-/-}$ mice exhibited increased mesor for *Bmal1*, *Clock*, and *Rev-Erb*α compared to *Taar5*$^{+/+}$ controls in the olfactory bulb (Figure 1B; Table 1). Whereas, *Taar5*$^{-/-}$ mice exhibited advanced acrophase in *Cry1* and *Per2* compared to *Taar5*$^{+/+}$ controls in the olfactory bulb (Figure 1B; Table 1). There is also some reorganization of circadian gene expression in the liver (Figure 1C) and gonadal white adipose tissue (Figure 1D; Table 1), albeit modest. In the liver, *Taar5*$^{-/-}$ mice had normal circadian gene expression, when compared to *Taar5*$^{+/+}$ controls (Figure 1C; Table 1). In gonadal WAT, the amplitude of *Bmal1* was increased and acrophase of *Bmal1* was delayed in *Taar5*$^{-/-}$ mice, whereas only the acrophase of Per2 was advanced in *Taar5*$^{-/-}$ mice compared to *Taar5*$^{+/+}$ controls (Figure 1D; Table 1). Given the key role that the TMAO pathway plays in suppressing the beiging of WAT[13], we also examined the expression of PR/SET domain 16 (Prdm16) and uncoupling protein 1 (Ucp1). *Taar5*$^{-/-}$ mice had increased mesor and advanced acrophase of Prdm16, yet no difference was detected in Ucp1, compared to *Taar5*$^{+/+}$ controls (Figure 1D; Table 1). *Taar5*$^{-/-}$ mice have unaltered oscillations in body weight (Figure 1 - figure supplement 1; Table 1).

We next examined circadian oscillations in circulating metabolite, hormone, and cytokine levels in *Taar5*$^{+/+}$ and *Taar5*$^{-/-}$ mice (Figure 1 – figure supplement 2; Table 1). When we measured substrates for gut microbial TMA production we found that *Taar5*$^{-/-}$ mice had normal oscillations in choline and *L*-carnitine (Figure 1 - figure supplement 2A; Table 1). However, there was a modest yet significant advance in the acrophase of plasma γ-butyrobetaine in *Taar5*$^{-/-}$ mice (Figure 1 - figure supplement 2A; Table 1). *Taar5*$^{-/-}$ mice also had slightly increased levels of TMA at ZT22, when compared to *Taar5*$^{+/+}$ controls (Figure 1 - figure supplement 2A; Table 1). However, TMA and TMAO levels were not significantly altered in *Taar5*$^{-/-}$ mice (Figure 1 - figure supplement 2A; Table 1). Interestingly, *Taar5*$^{-/-}$ mice had altered rhythmic levels in some but not all host metabolic hormones. Although, the circadian oscillations of plasma insulin and C-peptide were not significantly altered, *Taar5*$^{-/-}$ mice had a delay in acrophase of plasma glucagon, yet advanced

acrophase of glucagon-like peptide 1 (GLP-1), compared to *Taar5*$^{+/+}$ controls (Figure 1 - figure supplement 2B; Table 1). *Taar5*$^{-/-}$ mice also exhibited increased mesor for plasma leptin levels compare to wild-type controls (Figure 1 - figure supplement 2B; Table 1). *Taar5*$^{-/-}$ mice also had modest differences in circulating cytokines including a decrease in the mesor of monocyte chemoattractant 1 (MCP-1) and tumor necrosis factor α (TNFα) (Figure 1 - figure supplement 2B; Table 1) Collectively, these data demonstrate that *Taar5*$^{-/-}$ mice have altered circadian-related gene expression that is most apparent in the olfactory bulb (Figure 1; Table 1), and abnormal circadian oscillations in some but not all circulating hormones and cytokines (Figure 1 - figure supplement 2; Table 1).

We next set out to comprehensively analyze the circadian rhythms in behavioral phenotypes in mice lacking the TMA receptor TAAR5. In this line of investigation we took a very broad approach to examine impacts of *Taar5* deficiency on metabolic, cognitive, motor, anxiolytic, social, olfactory and innate behaviors. The main rationale behind this in-depth investigation was to allow for comparison to our recent work showing that pharmacologic blockade of the production of the TAAR5 ligand TMA (using choline TMA lyase inhibitors) produced clear metabolic, innate, and olfactory-related social behavioral phenotypes, but did not dramatically impact aspects of cognition, motor, or anxiolytic behaviors.[33,46]. Also, it is important to note other groups have recently shown that TAAR5 activation with non-TMA ligands or genetic deletion of *Taar5* results in clear olfactory[48-51], anxiolytic[51], cognitive[52], and sensorimotor[53,54] behavioral abnormalities. Here, it was our main goal to identify whether any behavioral phenotypes that were consistently seen in mice lacking bacterial TMA production[33,46] or host TMA sensing by TAAR5 (studied here) are time-of-day dependent indicating circadian inputs. Given the consistent alterations in innate and olfactory-related phenotypes seen in both mice lacking bacterial TMA production[33,46] and mice lacking host TMA sensing by TAAR5[47-54], we next followed up to perform select innate and olfactory-related behavioral tests in mice at defined circadian time

points (Figure 2).

To study the circadian presentation of phenotype, we carefully controlled the time window of testing for either the olfactory cookie test or marble burying test, both of which have been shown to be altered in mice lacking bacterial TMA synthesis[46,55]. When the olfactory cookie test was performed during the mid light cycle (ZT5-ZT7), the latency to find the buried cookie was significantly increased in male *Taar5*$^{-/-}$ mice compared to *Taar5*$^{+/+}$ controls (Figure 2A). However, when the same mice performed the olfactory cookie test at the dark-to-light phase transition (ZT23-ZT1), or at the light-to-dark phase transition (ZT13-ZT15), there were no significant differences between *Taar5*$^{+/+}$ and *Taar5*$^{-/-}$ mice (Figure 2A). When subjected to the marble burying test, only female *Taar5*$^{-/-}$ mice buried significantly more marbles than female wild-type controls only at ZT5-ZT7, but this was not apparent at other ZT timepoints (Figure 2B). Collectively, these data demonstrate that *Taar5*$^{-/-}$ mice exhibit highly gender-specific alterations in innate and olfactory behaviors, and these behavior phenotypes are only apparent at certain periods within the light cycle (Figures 2, and S2).

Although *Taar5*$^{-/-}$ mice showed time-dependent alterations in the olfactory cookie test, olfactory discrimination towards other diverse single stimuli such as banana, corn oil, almond, water, or social cues were not significantly altered (Figure 2 - figure supplement 1). When we subjected *Taar5*$^{-/-}$ mice to a battery of social behavioral tests, there were test-specific alterations that occur in a sexually dimorphic manner. All mouse groups (*Taar5*$^{+/+}$, *Taar5*$^{-/-}$, male and female) displayed no initial chamber bias in the initial trial of the three-chamber test (Figure 2- figure supplement 2A). In the three-chamber preference test, only male *Taar5*$^{-/-}$ mice showed no preference between an inanimate object and a social stimuli interaction (Figure 2 - figure supplement 2B). When subjected to the three-chamber social novelty test box , both male and female *Taar5*$^{-/-}$ mice showed no preference between the novel and familiar stimuli (Figure 2 - figure supplement 2C). In the social interaction with a juvenile mouse test, *Taar5*$^{-/-}$ females showed no significant

difference in interaction time between the initial interaction trial and the recognition trial four days later (Figure 2 - figure supplement 2D). In addition to alterations in social interactions, *Taar5*$^{-/-}$ mice also showed sexually dimorphic alterations in several other innate behavioral tests (Figure 2 - figure supplement 3). Female *Taar5*$^{-/-}$ mice exhibited a significantly higher startle response at 90, 100, 110, and 120 decibels (Figure 2 - figure supplement 3A), and significantly weaker forelimb grip strength (Figure 2 - figure supplement 3B) compared to *Taar5*$^{+/+}$ controls. When both sexes are combined there is a significant increase in the latency to withdraw during the hotplate sensitivity test in *Taar5*$^{-/-}$ mice compared to controls (Figure 2 - figure supplement 3C). Furthermore, both male and female *Taar5*$^{-/-}$ mice have slightly increased latency to fall during the rotarod test (Figure 2 - figure supplement 3D). Also, female but not male *Taar5*$^{-/-}$ mice exhibit reduced nest building compared *Taar5*$^{+/+}$ mice (Figure 2 - figure supplement 3E).

We next comprehensively examined cognitive, depression, and anxiety-like behaviors in *Taar5*$^{+/+}$ and *Taar5*$^{-/-}$ mice (Figure 2 - figure supplements 4 and 5). Both male and female *Taar5*$^{-/-}$ mice performed similarly to *Taar5*$^{+/+}$ controls in the open field, elevated plus maze, and Y-maze tests (Figure 2 - figure supplement 4B-D). However, female, but not male, *Taar5*$^{-/-}$ mice showed significantly reduced freezing compared to *Taar5*$^{+/+}$ controls in the cued fear conditioning test (Figure 2 - figure supplement 4A). When subjected to the Morris water maze, there were only minor alterations found in *Taar5*$^{-/-}$ mice. All mice showed similar latency to the platform. Male *Taar5*$^{-/-}$ mice showed increased distance traveled compared to wild-type controls, yet females were more similar to *Taar5*$^{+/+}$ controls (Figure 2 – figure supplement 5). However, female *Taar5*$^{-/-}$ mice showed increased velocity compared to *Taar5*$^{+/+}$ mice during the last 3 days of testing (Figure 2 - figure supplement 5). Collectively, the impact of *Taar5* deficiency on cognitive, depression, and anxiety-like behaviors was very modest.

Given the TMAO pathway has been linked to the beiging of white adipose tissue, and energy expenditure[13], we next examined circadian rhythms in energy metabolism during a cold challenge

and gene expression in thermogenic brown adipose tissue (BAT) in *Taar5*$^{-/-}$ mice (Figure 2 - figure supplement 6). Although male *Taar5*$^{-/-}$ mice showed unaltered oxygen consumption at thermoneutrality (30°C), room temperature (22°C), and during cold (4°C) exposure, female *Taar5*$^{-/-}$ mice had significantly elevated oxygen consumption that appeared most significant during the light cycle periods (Figure 2 - figure supplement 6A). To follow up we collected BAT from *Taar5*$^{+/+}$ and *Taar5*$^{-/-}$ mice at ZT2 (early light cycle) and ZT14 (early dark cycle) to examine potential alterations in circadian gene expression. Both male and female *Taar5*$^{-/-}$ mice showed marked upregulation of *Arntl1/Bmal1*, yet other than increased *Per1* expression at ZT14 all other circadian genes were largely unaltered in *Taar5*$^{-/-}$ mice (Figure 2 - figure supplement 6B). Taken together, all behavioral data presented here show that mice lacking *Taar5* have select sexually dimorphic alterations in olfactory, innate, social, and metabolic phenotypes.

Host TAAR5 Regulates the Circadian Rhythmicity of the Gut Microbiome

Bi-directional microbe-host communication is required for homeostatic control of chronobiology in the metaorganism.[56-60] Our data strongly suggest that gut microbe-derived TMA can shape host circadian rhythms in metabolic homeostasis and behavior[33,46], but we also wanted to test whether host TAAR5 may reciprocally regulate circadian rhythms of the gut microbiome[58,59]. The rationale for studying alterations in the gut microbiome stems from that fact that several previous studies show that manipulating the TMAO pathway at different levels (diet, microbe, and host) strongly alters gut microbiota in unexpected ways[7,11,31,33]. For example, provision of dietary substrates (i.e. choline or *L*-carnitine) or exogenous TMAO itself can reorganize gut microbial communities in mice[7,11]. Also, small molecule enzyme inhibitors blocking the bacterial production of TMA profoundly alter the cecal microbiome[31,33], and some of the anti-obesity and circadian rhythm altering effects can be transmitted by cecal microbial tranplantation[33]. Therefore, we examined the circadian oscillation in the cecal microbiome in *Taar5*$^{+/+}$ and *Taar5*$^{-/-}$ mice over a 24-hour period,

and found there were clear alterations that were time of day dependent (Figure 3 and Figure 3 – figure supplements 1 and 2; Table 1). At the phylum level, wild-type mice showed a modest decrease in the light cycle (i.e. ZT2-ZT10), and progressive loss of *Firmicutes* over the dark cycle (i.e. from ZT14-ZT22). In contrast, *Taar5*$^{-/-}$ mice showed a reciprocal increase during the light cycle, and more modest dip during the light cycle in Firmicutes (Figure 3 - figure supplement 1; Table 1). When we examined microbiome alterations at the genus level, there were much clearer alterations in specific bacteria (Figure 3; Figure 3 - figure supplement 2; Table 1). In particular, the acrophase of several *Lachnospiraceae, Odoribacter*, and *Dubosiella* genera are altered in *Taar5*$^{-/-}$ mice when compared to wild-type controls (Figure 3; Figure 3 - figure supplement 2; Table 1). Although there were many microbiome alterations, *Taar5*$^{-/-}$ mice showed delayed acrophase for *Lachnospiraceae UCG-002*, *Lachnospiraceae NK4A136*, *Desulfovibrio*, *Bacteroides*, *Dubosiella*, *Colidextribacter, Alistipes, Turicibacter, Muribaculum, Helicobacter, and Parabacteroides,* when compared to *Taar5*$^{+/+}$ mice (Figure 3 - figure supplement 2; Table 1). Other genera such as *Lachnospiraceae UCG-006*, *Odoribacter*, *Butyricicoccus*, *Coriobacteriaceae UCG-002*, *Acetatifactor*, and *A2* showed advanced acrophase in *Taar5*$^{-/-}$ mice (Figure 3 - figure supplement 2; Table 1). It is important to note that previous independent studies have also shown that either blocking bacterial TMA synthesis[33] or FMO3-driven TMA oxidation[29] can also strongly reorganize the gut microbiome in mice. Although more work is needed to fully understand the underlying mechanisms, it is clear that both gut microbe-driven TMA production and host sensing of TMA by TAAR5 (Figures 3; Figure 3 - figure supplement 2; Table 1) can strongly impact on circadian oscillations of the gut microbiome.

Mice Genetically Lacking Either Gut Microbial TMA Production or Host-Driven TMA Oxidation Have Altered Circadian Rhythms

To confirm and extend the idea that gut microbe-derived TMA can shape host circadian rhythms

we next performed experiments where we genetically deleted either gut microbial TMA synthesis or host-driven TMA oxidation. First, we used gnotobiotic mice engrafted with a defined microbial community with or without genetic deletion of the choline TMA lyase CutC (i.e. *Clostridium sporogenes* wild-type versus Δ*cutC*) to understand the ability of gut microbe-derived TMA to alter host circadian rhythms (Figure 4; Figure 4 – figure supplement 1; Figure 4 – figure supplement 2). Circadian oscillations in plasma TMA and TMAO that peak in the early dark cycle are only detectable in the group colonized with *C. sporogenes* (WT), but not Δ*cutC C. sporogenes* (Figure 4A). Other TMAO pathway-related metabolites including choline, *L*-carnitine, γ-butyrobetaine, and betaine also exhibited modest alterations in circadian rhythms (Figure 4A). Mice lacking choline TMA lyase activity showed modestly reduced mesor in plasma choline, and advanced acrophase in both plasma betaine and γ-butyrobetaine (Figure 4A; Table 1). In a similar manner to *Taar5*$^{-/-}$ mice (Figure 1), mice colonized with Δ*cutC C. sporogenes* show alterations in the expression of some but not all circadian genes in the olfactory bulb (Figure 4B; Table 1). Mice colonized with Δ*cutC C. sporogenes* had significantly advanced acrophase for *Arntl/Bmal1*, yet delayed acrophase for Clock, in the olfactory bulb when compared to mice colonized with the control community (Figure 4B; Table 1). However, the oscillatory pattern of other circadian genes were not significantly altered. When we examined circulating hormones and cytokines, there were clear alterations in the circadian oscillation in mice genetically lacking choline TMA lyase activity (Figure 4C; Table 1). Mice colonized with the Δ*cutC C. sporogenes* community exhibited delayed acrophase for plasma insulin and interleukins 2 (IL-2) and 33 (IL-33) when compared to mice harboring the wild-type community that could produce TMA (Figure 4C; Table 1). Mice lacking choline TMA lyase activity also had an advanced acrophase for GLP-1, leptin, and IL-1β (Figure 2C; Table 1). It is interesting to note that we examined the cecal abundance of the five bacterial strains in our defined community, there were clear alterations

that were time of day dependent (Figure 4 - figure supplement 1). Four of the bacterial strains (*C. sporogenes*, *B. theta*, *B. caccae*, and *B. ovatus*) showed clear circadian oscillations when a zero amplitude test was performed in mice colonized with wild-type community. However, the community lacking *cutC* lost all significant circadian oscillation of these same four bacterial strains (Figure 4 - figure supplement 1; Table 1), showing that bacterial production of TMA can broadly impact both microbe-microbe and microbe-host interactions in circadian rhythms.

To follow up on our previous findings that FMO3 suppresses both beige and brown fat-induced cold induced thermogenesis[13], we also wanted to examine circadian patterns in subscapular brown adipose tissue (BAT) of Δ*cutC C. sporogenes*-colonized mice (Figure 4 - figure supplement 2; Table 1). Although there were no statistically-significant alterations in circadian gene expression in the BAT isolated from Δ*cutC C. sporogenes*-colonized mice, the acrophase of phosphatidylethanolamine methyltransferase (*Pemt*) was delayed in mice colonized with the Δ*cutC* community compared to mice colonized with the control wild-type community (Figure 4 - figure supplement 2A; Table 1). We next wanted more comprehensively quantify a variety of other well-known metabolites that are known to originate from bacterial sources (Figure 4 - figure supplement 2B). The rationale for performing microbe-focused metabolomics is that we have found if we alter one gut microbe-derived metabolite in other gnotobiotic mouse studies, there can be unexpected alterations in other distinct classes of microbe-derived metabolites[61]. This is likely due to the fact that complex microbe-microbe and microbe-host interactions work together to define systemic levels of circulating metabolites, influencing both the production and turnover of distinct and unrelated metabolites. Although the targeted deletion of *cutC* in *C. sporogenes* prevents the production of TMA from choline, there were alterations of several other gut microbe-derived metabolites in mice colonized with the *ΔcutC C. sporogenes* community (Figure 4 - figure supplement 2). Bacterially-derived aromatic amino acid metabolties such as hippuric acid, indole-3-propionic acid, and indole acetic acid were significantly reduced in mice colonized with

the Δ*cutC* community (Figure 4 - figure supplement 2). Also, the bacterially-derived phenylalanine metabolites phenylacetic acid and phenylacetylglycine gained rhymicity with marked increases in their peak amplitude in mice colonized with the Δ*cutC* community when compared to control mice (Figure 4 - figure supplement 2).

Finally, we wanted to examine whether host co-metabolism of TMA can also alter circadian rhythms (Figure 4 – figure supplement 2). Although gut microbes are the sole source of TMA, circulating levels are also shaped by abundant conversion of TMA to TMAO by the host liver enzyme FMO3[13,29]. To test whether the hepatic conversion of TMA to TMAO by FMO3 may alter circadian rhythms, we necropsied female *Fmo3*$^{+/+}$ and *Fmo3*$^{-/-}$ mice at ZT2 (early light cycle) or ZT14 (early dark cycle). *Fmo3*$^{-/-}$ mice have reduced levels of TMAO at both ZT2 and ZT14, as well as reduced expression of key circadian genes *Arntl* and *Per1* at ZT2 (Figure 4 – figure supplement 2). Taken together, our data suggest that bacterial production, FMO3-driven metabolism of TMA, as well as sensing of TMA by the host receptor TAAR5, converge to shape circadian rhythms in gene expression, metabolic hormones, gut microbiome composition, and innate behaviors.

Discussion

The metaorganismal TMAO pathway is strongly associated with many human diseases[5-29], which has prompted the rapid development of drugs intended to lower circulating levels of TMAO.[30-37] As the rapid drug discovery advances towards human studies, it will be extremely important to understand the diverse mechanisms by which the primary metabolite TMA and/or the secondary metabolite TMAO promotes disease pathogenesis in the human metaorganism. There is compelling evidence that the end product of the pathway TMAO can promote inflammation, ER stress and platelet activation via activation of NFκB, the NLRP3 inflammasome, PERK, and stimulus-dependent calcium release, respectively.[28,38-41] However, these TMAO-driven mechanisms only partially explain the links to so many diverse human

diseases. Here, we provide new evidence that in addition to these TMAO-driven mechanisms, the primary gut microbe TMA can in parallel shape circadian rhythms through the host GPCR TAAR5. The major findings of the current studies are: (1) Mice lacking the TMA receptor TAAR5 have abnormal oscillations in core circadian genes, particularly in the olfactory bulb, (2) Compared to wild-type controls, *Taar5*$^{-/-}$ mice have altered circulating levels of cytokines, metabolic hormones, and metabolites at certain times of the day, (3) *Taar5*$^{-/-}$ mice have altered innate and repetitive behaviors that emerge only in a time of day-dependent manner, (4) The normal oscillatory behavior of the cecal microbiome is dysregulated in *Taar5*$^{-/-}$ mice, (5) Genetic deletion of gut microbial choline TMA lyase activity, using defined *cutC*-null microbial communities *in vivo*, results in rewiring of circadian rhythms in gene expression, metabolic hormones, cytokines, and metabolites, (6) The bacterial strains in the defined microbial used in gnotobiotic mouse study oscillate differently depending on the presence of *cutC*, and (7) Mice lacking the host liver TMA-to-TMAO converting enzyme FMO3 likewise have altered circadian gene expression in the olfactory bulb. Collectively, our findings suggest that therapeutic strategies designed to limit gut microbial TMA production (i.e. TMA lyase inhibitors), host liver TMA oxidation (i.e. FMO3 inhibitors), or sensing of TMA by the host GPCR TAAR5 (i.e. TAAR5 inhibitors) will need to be carefully evaluated for pleiotropic effects on circadian rhythms. This body of work also demonstrates that diet-microbe-host interactions can powerfully shape chronobiology, and provides one of the first examples of a microbial metabolite being sensed by a host GPCR to rewire circadian rhythms.

Currently, the only known host receptor that senses gut microbe-produced TMA is the volatile amine receptor TAAR5, which allows for species-specific recognition of the “fishy” odor intrinsic to TMA but not TMAO.[47-49] In general, the trace amine-associated receptor (TAAR) subfamily of GPCRs primarily function as olfactory receptors in vertebrates.[49,50] Ligand-dependent activation of each individual TAAR receptor occurs in a unique sensory neuron population primarily

localized to olfactory cilia, and when activated typically elicit TAAR-specific olfactory-related behavior responses.[49,50] TMA-dependent activation of TAAR5 was first shown to promote attraction and social interaction between females and male mice in a very species and strain-specific manner.[48] This seminal study by Liberles and colleagues showed that the TMA-TAAR5 olfactory circuit can powerful shape olfactory-driven social interaction, and FMO3-driven conversion of TMA to TMAO suppresses TAAR5 activation.[48] In parallel, we recently performed a comprehensive study to assess cognitive, motor, anxiolytic, social, olfactory and innate behaviors in mice treated with small molecule choline TMA lyase inhibitors to block bacterial TMA production.[46] Much like the olfactory and social phenotypes seen in *Taar5*$^{-/-}$ mice[48], we found that pharmacologic blockade of bacterial TMA production significantly altered olfaction and olfactory-related social behaviors, but did not significantly alter cognitive, motor, anxiolytic behaviors[46]. It is interesting to note that choline TMA lyase inhibitors altered olfactory perception of several odorant stimuli beyond TMA itself including a cookie, almond, vanilla, corn oil, and coyote urine.[46] This indicates that drugs blocking TMA-TAAR5 signaling could impact olfactory neurogenesis to impact sensing of diverse odorant cues that are well beyond the rotten fish smell intrinsic to TMA. Given that anosmia is a common occurrence in several TMAO-related diseases including CKD[62], obesity, diabetes[63], neurodegenerative diseases[64,65], and COVID-19[66], it is tempting to speculate that TMA-lowering therapeutics may hold promise to potentially restore olfactory perception to diverse stimuli in these disease conditions. However, additional studies are needed to formally test this hypothesis. Given the clear links between the TMA-TAAR5 signaling axis and olfactory-related behaviors in mice[46,48], it will be important to carefully evaluate effects of TMAO-lowering drugs on olfaction in future human studies.

A commonality of many bacterially-derived volatile metabolites is that they have a pungent odor which is sensed by olfactory neurons, and these microbe-host olfactory circuits shape many diverse behavioral and metabolic responses in the human host. For example, strong bacterially-

derived odors such as trimethylamine (i.e. smells like rotting fish), hydrogen sulfide (i.e. the rotten egg smell), polyamines including putrescine and cadaverine (i.e. the smell of rotting cadavers/roadkill) can serve as an effective “don't eat me” signal for us to avoid consuming spoiled food. Within the human metaorganism, the gut microbiome and select gut microbe-derived metabolites play an important role in shaping not only food intake but also other aspects of host energy metabolism, insulin sensitivity, immunology, and the circadian clock.[56-60] It is important to note that there is bi-directional communication between gut microbes and the host in maintaining the circadian rhythms in metabolism and immunity within mammalian metaorganisms.[56-60] First, central and peripheral clock machinery in the host clearly shape circadian oscillations in the gut microbiome primarily through innate immune mechanisms.[56,57] At the same time, circadian oscillations intrinsic to the gut microbiome itself can have profound impacts on host physiology and disease.[58-60] Although there is extensive knowledge on how the host circadian clock can impact the oscillatory behavior of the gut microbiome[56,57], much less is known regarding mechanisms by which the gut microbiome can instruct the host circadian clock. Our data support the notion that gut microbe-derived TMA and TAAR5 activation can impact circadian rhythms in gene expression, metabolic hormones, gut microbiome composition, and innate behaviors. Using both pharmacologic[33] and genetic approaches, we have demonstrated that blocking either gut microbial TMA production or sensing by the host TMA receptor TAAR5 results in striking rearrangement of circadian rhythms in the gut microbiome that are linked to metabolic homeostasis and olfactory-related behaviors in mice[33,46]. In further support of the connections between the TMAO pathway and host circadian disruption, a recent paper showed that FMO3 inhibitors blocking host TMA oxidation improved learning and memory deficits driven by chronic sleep loss[67]. Other recent studies in humans also show that TMAO is elevated with sleep deprivation[68], and elevated TMAO levels are associated with an “evening chronotype” that is linked to increased risk of cardiometabolic disease.[69] Collectively, the metaorganismal TMAO

pathway plays an important in integrating dietary cues and microbe-host interactions in circadian rhythms. Given TMAO lowering drugs are rapidly advancing towards human studies, it will be of great interest to determine whether these drugs can improve circadian rhythms and potentially synergize with other developmental chronotherapies to improve human health.

Limitations

First, it is critically important to point out that the TMA-TAAR5 signaling axis has evolved to elicit species-specific behavioral responses that differ quite substantially across rodent species and humans.[48,49] When the "stinky" fish odor of TMA is sensed by rat or human TAAR5, the result is typically aversion from consuming what is perceived as rotting food.[48,49] However, select strains of mice have concentration-dependent attraction to low levels of TMA or aversion to high levels of TMA.[48] It has been theorized that this concentration-dependent behavioral response to TMA in mice may have evolved as a kairomone signal that allows mice to sense approaching prey animals.[48,49] Clearly the human TMA-TAAR5 signaling circuit evolved for different reasons, where predator-prey signaling circuits are less prominent. Therefore, additional studies are needed to better understand what diverse roles TMA-driven TAAR5 activation plays in the circadian rhythms in human metabolism and behavior. The recent discovery of humans with loss-of-function TAAR5 genetic variants[70] may provide a unique population to confirm and extend the findings we report here in mice. Another limitation in our current understanding is that drugs blocking gut microbial TMA production[30-37] or host TMA oxidation[13,15,67] have only been tested in mice. Although these drugs show clear benefit in mice models, the human gut microbiome is quite different than mice and the relative affinity of TMA for TAAR5 is ~ 200-fold less in humans when compared to rodent forms of the receptor.[47-49] Therefore, it is impossible to extrapolate finding in mice to humans. As TMAO lowering drugs move into human trials, there is strong potential that human-specific phenotypes may emerge. Another limitation is that we

have not rigorously studied diet-induced obesity, effects on food intake, or cardiovascular disease/atherosclerosis in this study. Additional studies are needed to understand whether TMA-driven TAAR5 activation impacts cardiometabolic disease. A final limitation here is that here we have studied mice globally lacking TAAR5 in all tissues and cell types. Although TAAR5 has primarily been studied in olfactory neurons in the brain, TAAR5 is also expressed in immune cells[71] as well as skeletal and cardiac muscle[33]. Given the expression of TAAR5 outside of the central nervous system, future studies utilizing cell-restricted *Taar5* knockout mice will provide clues into the cell autonomous roles for TMA-TAAR5 signaling. Despite these limitations, a growing body of evidence links TMA and TAAR5 activation to circadian regulation of metabolism and olfactory-related behaviors.

Lead contact

Further information and requests for resources and reagents should be directed to and will be fulfilled by the lead contact, J. Mark Brown (brownm5@ccf.org)

Materials availability

All the data and materials that support the findings of this study are available within the article. Additional details can be aquired via a direct request to the corresponding author.

Data and code availability

The 16S microbiome data from wild-type and *Taar5* knockout mice are publicly available at the following link: DOI 10.5281/zenodo.15802940.

Code used for cosinor analyses:

1. Sachs, M.C. (2014) cosinor: Tools for estimating and predicting the cosinor model, version 1.1. R package: https://CRAN.R-project.org/package=cosinor.

Any additional information required to reanalyze the data reported in this paper is available from the lead contact (Dr. J. Mark Brown) upon request

Acknowledgements

This work was supported in part by National Institutes of Health grants R01 DK130227 (J.M.B.), P01 HL147823 (J.M.B.), P50 AA024333 (J.M.B.), RF1 NS133812 (J.M.B.), and an American Heart Association Postdoctoral Fellowship 24POST1178494 (S.D.). We are grateful to Dr. Federico Rey (University of Wisconsin – Madison, USA) for providing bacterial strains used in the mouse gnotobiotic studies performed here. We are also grateful to Dr. Stan Hazen for providing access to mass spectrometer instruments dedicated to targeted metabolomic methods necessary to quantify diverse gut microbe-derived metabolites.

Author Contributions

Conceptualization, K.M. and J.M.B.; methodology, K.M., W.J.M., D.O., A.L.B., T.J., A.C.B., A.J.H., S.D., M.M., N.M., V.V., L.J.O., X.Y., D.M.Y., N.Z., R.H., R.B., P.L., D.L., A.M.H., N.S., M.D., J.A.B., and G.R.S., Z.W; investigation, K.M., W.J.M., D.O., A.L.B., T.J., A.C.B., A.J.H., S.D., M.M., N.M., V.V., L.J.O., X.Y., D.M.Y., N.Z., R.H., R.B., P.L., D.L., N.S., M.D., J.A.B., and Z.W; validation, K.M., W.J.M., A.C.B., A.J.H., S.D., M.M., L.J.O., R.B., P.L., D.L., N.S., M.D., J.A.B., and Z.W; formal analysis, K.M., W.J.M., N.S., T.G., G.R.S., Z.W., J.M.B; writing – original draft, K.M. and J.M.B.; writing – reviewing and editing, K.M., W.J.M., D.O., A.L.B., T.J., A.C.B., A.J.H., S.D., M.M., N.M., V.V., L.J.O., X.Y., D.M.Y., N.Z., R.H., R.B., P.L., D.L., A.M.H., N.S., M.D., J.A.B., G.R.S., and Z.W.; funding acquisition, J.M.B.; supervision, J.M.B.

Declaration of interests

Competing interests: Z.W. reports being named as co-inventor on pending and issued patents held by the Cleveland Clinic relating to cardiovascular diagnostics and therapeutics. Z.W. also reports having received royalty payments for inventions or discoveries related to cardiovascular diagnostics or therapeutics from Cleveland Heart Lab, a fully owned subsidiary of Quest Diagnostics and Procter & Gamble. C.M.T. consults for Abbott Laboratories. J.M.B. reports being named as co-inventor on pending and issued patents held by the Cleveland Clinic relating to choline trimethylamine lyase inhibitors as therapies for cardiometabolic disease including obesity and type 2 diabetes. All other authors: K.M., W.J.M., D.O., A.L.B., T.J., A.C.B., A.H., S.D., M.M., N.M., V.V., L.J.O., X.Y., D.M.Y., N.Z., R.H., R.B., P.L., D.L., N.S., T.G., M.D., J.A.B., and G.R.S. have no competing interests.

REFERENCES

1. Aron-Wisnewsky, J., and Clément, K. (2016) The gut microbiome, diet, and links to cardiometabolic and chronic disorders. Nat Rev Nephrol. *12,* 169-181.

2. Nobs, S.P., Zmora, N., Elinav, E. (2020) Nutrition regulates innate immunity in health and disease. Annu Rev Nutr. *40,* 189-219.

3. Arora, T., and Bäckhed, F. (2016) The gut microbiota and metabolic disease: current understanding and future perspectives. J. Intern. Med. *280,* 339-349.

4. Valles-Colomer, M., Menni, C., Berry, S.E., Valdes, A.M., Spector, T.D., and Segata, N. (2023) Cardiometabolic health, diet and the gut microbiome: a meta-omics perspective. Nat Med. *29,* 551-561.

5. Wang, Z., Klipfell, E., Bennett, B.J., Koeth, R., Levison, B.S., Dugar, B., Feldstein, A.E., Britt, E.B., Fu, X., Chung, Y.M., et al. (2011). Gut flora metabolism of phosphatidylcholine promotes cardiovascular disease. Nature *472,* 57-63.

6. Tang, W.H., Wang, Z., Levison, B.S., Koeth, R.A., Britt, E.B., Fu, X., Wu, Y., and Hazen, S.L. (2013) Intestinal microbial metabolism of phoaphatidylcholine and cardiovascular risk. N. Engl. J. Med. *368,* 1575-1584.

7. Koeth, R.A., Wang, Z., Levison, B.S., Buffa, J.A., Org, E., Sheehy, B.T., Britt, E.B., Fu, X., Wu, Y., Li, L., et al. (2013) Intestinal microbiota metabolism of L-carnitine, a nutrient in red meat, promotes atherosclerosis. Nat. Med.*19,* 576-585.

8. Zhu, W., Gregory, J.C., Org, E., Buffa, J.A., Gupta, N., Wang, Z., Li, L., Fu, X., Wu, Y., Mehrabian, M., et al. (2016) Gut microbial metabolite TMAO enhances platelet hyperreactivity and thrombosis risk. Cell *165,* 111-124.

9. Skye, S.M., Zhu, W., Romano, K.A., Guo, C.J., Wang, Z., Jia, X., Kirsop, J., Haag, B., Lang, J.M., DiDonato, J.A., et al. (2018) Microbial transplantation with human gut commensals containing CutC is sufficient to transmit enhanced platelet reactivity and thrombosis potential. Circ. Res. 12*3,* 1164-1176.

10. Bennett, B.J., de Aguiar Vallim, T.Q., Wang, Z., Shih, D.M., Meng, Y., Gregory, J., Allayee, H., Lee, R., Graham, M., Crooke, R., et al. (2013) Trimethylamine-N-oxide, a metabolite associated with atherosclerosis, exhibits complex genetic and dietary regulation. Cell Metab. *17,* 49-60.

11. Koeth, R.A., Levison, B.S., Culley, M.K., Buffa, J.A., Wang, Z., Gregory, J.C., Org, E., Wu, Y., Li, L., Smith, J.D., et al. (2014) gamma-Butyrobetaine is a proatherogenic intermediate in gut microbial metabolism of L-carnitine to TMAO. Cell Metab. *20,* 799-812.

12. Leng, X., Wei, X., Wang, J., Yao, X., Zhang, M., Sun, D., Liang, J., Chi, L., and Cheng, Y. (2025) Impacts of intestinal microbiota metabolite trimethylamine N-oxide on cardiovascular disease: a bibliometric analysis. Front. Microbiol. *15,* 1491731.

13. Schugar, R.C., Shih, D.M., Warrier, M., Helsley, R.N., Burrows, A., Ferguson, D., Brown, A.L., Gromovsky, A.D., Heine, M., Chatterjee, A., et al. (2017) The TMAO-producing enzyme flavin-containing monooxygenase 3 regulates obesity and the beiging of white adipose tissue. Cell Rep. *20,* 279.

14. Dehghan, P., Farhangi, M.A., Nikniaz, L., Nikniaz, Z., and Asghari-Jafarabadi, M. (2020) Gut microbiota-derived metabolite trimethylamine N-oxide (TMAO) potentially increases the risk of obesity in adults: an exploratory systematic review and dose-response meta-analysis. Obes. Rev. *21,* e12993.

15. Miao, J., Ling, A.V., Manthena, P.V., Gearing, M.E., Graham, M.J., Crooke, R.M., Croce, K.J., Esquejo, R.M., Clish, C.B.; Morbid Obesity Study Group; et al. (2015) Flavin-containing monooxygenase 3 as a potential player in diabetes-associated atherosclerosis. Nat. Commun. *6,* 6498.

16. Steinke, I., Ghanei, N., Govindarajulu, M., Yoo, S., Zhong, J., and Amin, R.H. (2020) Drug discovery and development of novel therapeutics for inhibiting TMAO in models of atherosclerosis and diabetes. Front Physiol. *11,* 567899.

17. Tang, W.H., Wang, Z., Kennedy, D.J., Wu, Y., Buffa, J.A., Agatisa-Boyle, B., Li, X.S., Levison, B.S., and Hazen, S.L. (2015) Gut microbiota-dependent trimethylamine N-oxide (TMAO) pathway contributes to both development of renal insufficiency and mortality risk in chronic kidney disease. Circ Res. *116,* 448-455.

18. Zixin, Y., Lulu, C., Xiangchang, Z., Qing, F., Binjie, Z,, Chunyang, L,, Tai, R,, and Dongsheng, O. (2022) TMAO as a potential biomarker and therapeutic target for chronic kidney disease: a review. Front Pharmacol. *13,* 929262.

19. Kumari, S., Goyal, V., Kumaran, S.S., Dwivedi, S.N., Srivastava, A., and Jagannathan, N.R. (2020) Quantitative metabolomics of saliva using proton NMR spectroscopy in patients with Parkinson's disease and healthy controls. Neurol Sci. *41,* 1201-1210.

20. Vogt, N.M., Romano, K.A., Darst, B.F., Engelman, C.D., Johnson, S.C., Carlsson, C.M., Asthana, S., Blennow, K., Zetterberg, H., Bendlin, B.B., and Rey, F.E. (2018) The microbiota-derived metabolite trimethylamine N-oxide is elevated in Alzheimer's disease. Alzheimers Res. Ther. *10,* 124.

21. Xu, R., Wang, Q., and Li, L. (2015) A genome-wide systems analysis reveals strong link between colorectal cancer and trimethylamine N-oxide (TMAO), a gut microbial metabolite of dietary red meat and fat. BMC Genomics *Suppl 7,* S4.

22. Banerjee, R., Wehrle, C.J., Wang, Z., Wilcox, J.D., Uppin, V., Varadharajan, V., Mrdjen, M., Hershberger, C., Reizes, O., Yu, J.S., et al. (2024) Circulating gut microbe-derived metabolites are associated with hepatocellular carcinoma. Biomedicines *12,* 1946.

23. Li, D., Lu, Y., Yuan, S., Cai, X., He, Y., Chen, J., Wu, Q., He, D., Fang, A., Bo, Y., et al. (2022) Gut microbiota-derived metabolite trimethylamine-N-oxide and multiple health outcomes: an umbrella review and updated meta-analysis. Am. J. Clin. Nutr. *116,* 230-243.

24. Heianza, Y., Ma, W., Manson, J.E., Rexrode, K.M., and Qi, L. (2017) Gut microbiota metabolites and risk of major adverse cardiovascular disease events and death: a systematic review and meta-analysis of prospective studies. J Am Heart Assoc. *6,* e004947.

25. Schiattarella, G.G., Sannino, A., Toscano, E., Giugliano, G., Gargiulo, G., Franzone, A., Trimarco, B., Esposito, G., and Perrino C. (2017) Gut microbe-generated metabolite trimethylamine-N-oxide as cardiovascular risk biomarker: a systematic review and dose-response meta-analysis. Eur. Heart J. *38,* 2948-2956.

26. Jia, J., Dou, P., Gao, M., Kong, X., Li, C., Liu, Z., and Huang, T. (2019) Assessment of causal direction between gut microbiota-dependent metabolites and cardiometabolic health: a bidirectional Medelian Randomization analysis. Diabetes *68,* 1747-1755.

27. Zhou, H., Luo, Y., Zhang, W., Xie, F., Deng, C., Zheng, W., Zhu, S., and Wang, Q. (2023) Causal effect of gut-microbiota-derived metabolite trimethylamine N-oxide on Parkison's disease: A Mendelian randomization study. Eur. J. Neurol. *30,* 3451-3461.

28. Chen, S., Henderson, A., Petriello, M.C., Romano, K.A., Gearing, M., Miao, J., Schell, M., Sandoval-Espinola, W.J., Tao, J., Sha, B., et al. (2019) Trimethylamine N-oxide binds and activates PERK to promote metabolic dysfunction. Cell Metab. *30,* 1141-1151.

29. Zhu, W., Buffa, J.A., Wang, Z., Warrier, M., Schugar, R., Shih, D.M., Gupta, N., Gregory, J.C., Org, E., Fu, X., et al. (2018) Flavin monooxygenase 3, the host hepatic enzyme in the metaorganismal trimethylamine N-oxide-generating pathway, modulates platelet responsiveness and thrombosis risk. J. Thromb. Haemost. *16,* 1857-1872.

30. Wang, Z., Roberts, A.B., Buffa, J.A., Levison, B.S., Zhu, W., Org, E., Gu, X., Huang, Y., Zamanian-Daryoush, M., Culley, M.K, et al. (2015) Non-lethal inhibition of gut microbial trimethylamine production for the treatment of atherosclerosis. Cell *163,* 1585-1595.

31. Roberts, A.B., Gu, X., Buffa, J.A., Hurd, A.G., Wang, Z., Zhu, W., Gupta, N., Skye, S.M., Cody, D.B., Levison, B.S., et al. (2018) Development of a gut microbe-targeted nonlethal therapeutic to inhibit thrombosis potential. Nat. Med. 24, 1407-1417.

32. Organ, C.L., Li, Z., Sharp, T.E. 3rd, Polhemus, D.J., Gupta, N., Goodchild, T.T., Tang, W.H.W., Hazen, S.L., and Lefer, D.J. (2020) Nonlethal inhibition of gut microbial trimethylamine N-oxide production improves cardiac function and remodeling in a murine model of heart failure. J Am Heart Assoc. *9,* e016223.

33. Schugar, R.C., Gliniak, C.M., Osborn, L.J., Massey, W., Sangwan, N., Horak, A., Banerjee, R., Orabi, D., Helsley, R.N., Brown, A.L., et al. (2022) Gut microbe-targeted choline trimethylamine lyase inhibition improves obesity via rewiring of host circadian rhythms. Elife *11,* e63998.

34. Helsley, R.N., Miyata, T., Kadam, A., Varadharajan, V., Sangwan, N., Huang, E.C., Banerjee, R., Brown, A.L., Fung, K.K., Massey, W.J., et al. (2022) Gut microbial trimethylamine is elevated in alcohol-associated hepatitis and contributes to ethanol-induced liver injury in mice. Elife *11,* e76554.

35. Zhang, W., Miikeda, A., Zuckerman, J., Jia, X., Charugundla, S., Zhou, Z., Kaczor-Urbanowicz, K.E., Magyar, C., Guo, F., Wang, Z., et al. (2021) Inhibition of microbiota-dependent TMAO production attenuates chronic kidney diease in mice. Sci. Rep. *11,* 518..

36. Gupta, N., Buffa, J.A., Roberts, A.B., Sangwan, N., Skye, S.M., Li, L., Ho, K.J., Varga, J., DiDonato, J.A., Tang, W.H.W., and Hazen, S.L.(2020) Targeted inhibition of gut microbial trimethylamine N-oxide production reduces renal tubulointerstitial fibrosis and functional impairment in a murine model of chronic kidney disease. Arterioscler. Thromb. Vasc. Biol. *40,* 1239-1255.

37. Benson, T.W., Conrad, K.A., Li, X.S., Wang, Z., Helsley, R.N., Schugar, R.C,, Coughlin, T.M., Wadding-Lee, C., Fleifil, S., Russell, H.M., et al. (2023) Gut microbiota-derived trimethylamine N-oxide contributes to abdominal aortic aneurysm through inflammatory and apoptotic mechanisms. Circulation *147,* 1079-1096.

38. Seldin, M.M., Meng, Y., Qi, H., Zhu, W., Wang, Z., Hazen, S.L., Lusis, A.J., and Shih, D.M. (2016) Trimethylamine N-oxide promotes vascular inflammation through signaling of mitogen-activated protein kinase and nuclear factor-kB. J. Am. Heart Assoc. *5,* e002767.

39. Sun, X., Jiao, X., Ma, Y., Liu, Y., Zhang, L., He, Y., and Chen, Y. (2016) Trimethylamine N-oxide induces inflammation and endothelial dysfunction in human umbilical vein endothelial cells via activating ROS-TXNIP-NLRP3 inflammasome. Biochem. Biophys. Res. Commun. *481,* 63-70.

40. Chen, M.L., Zhu, X.H., Ran, L., Lang, H.D., Yi, L., and Mi, M.T.(2017) Trimethylamine-N-oxide induces vascular inflammation by activating the NLRP3 inflammasome through the SIRT3-SOD2-mtROS signaling pathway. J. Am. Heart Assoc. *6,* e006347.

41. Zhang, X., Li, Y., Yang, P., Liu, X., Lu, L., Chen, Y., Zhong, X., Li, Z., Liu, H., Ou, C., et al. (2020) Trimethylamine-N-oxide promotes vascular calcification through activation of NLRP3 (Nucleotide-Binding Domain, Leucine-Rich-Containing Family, Pyrin Domain-Containing-3) inflammasome and NF-kB (Nuclear Factor kB) signals. Arterioscler. Thromb. Vasc. Biol. *40,* 751-765.

42. Sulli, G., Manoogian, E.N.C., Taub, P.R., and Panda, S. (2018) Training the circadian clock, clocking the drugs, and drugging the clock to prevent, manage, and treat chronic disease. Trends Pharmacol. Sci. *39,* 812-827.

43. Bolshette, N., Ibrahim, H., Reinke, H., and Asher, G. (2023) Circadian regulation of liver function: from molecular mechanisms to disease pathophysiology. Nat. Rev. Gastroenterol. Hepatol. *20,* 695-707.

44. Zheng, D., Ratiner, K., and Elinav, E. (2020) Circadian influences of diet on the microbiome and immunity. Trends Immunol. *41,* 512-530.

45. Bishehsari, F., Voigt, R.M., and Keshavarzian, A. (2020) Circadian Rhythms and the gut microbiota: from the metabolic syndrome to cancer. Nat. Rev. Endocrinol. *16,* 731-739.

46. Massey, W.J., Kay, K.E., Jaramillo, T.C., Horak, A.J. 3rd, Cao, S., Osborn, L.J., Banerjee, R., Mrdjen, M., Hamoudi, M.K., Silver, D.J.,et al. (2023) Metaorganismal choline metabolism shapes olfactory perception. J. Biol. Chem. *299,* 105299.

47. Wallrabenstein, I., Kuklan, J., Weber, L., Zborala, S., Werner, M., Altmüller, J., Becker, C., Schmidt, A., Hatt, H., Hummel, T., and Gisselmann, G. (2013) Human trace amine-associated receptor TAAR5 can be activated by trimethylamine. PLoS One *8,* e54950.

48. Li, Q., Korzan, W.J., Ferrero, D.M., Chang, R.B., Roy, D.S., Buchi, M., Lemon, J.K., Kaur, A.W., Stowers, L., Fendt, M., and Liberles, S.D. (2013) Synchronous evolution of an odor biosynthesis pathway and behavioral response. Curr. Biol. *23,* 11-20.

49. Liberles, S.D. (2015) Trace amine-associated receptors: ligands, neural circuits, and behaviors. Curr. Opin. Neurobiol. *34* 1-7.

50. Freyberg, Z., and Saavedra, J.M. (2020) Trace amines and trace amine-associated receptors: A new frontier in cell signaling. Cell. Mol. Neurobiol. *40,* 189-190.

51. Espinoza, S., Sukhanov, I., Efimova, E.V., Kozlova, A., Antonova, K.A., Illiano, P., Leo, D., Merkulyeva, N., Kalinina, D., Musienko, P., et al. (2020) Trace amine-associated receptor 5 provides olfactory input into limbic brain areas and modulates emotional behaviors and serotonin transmission. Front. Mol. Neurosci. *13,* 18.

52. Maggi, S., Bon, C., Gustincich, S., Tucci, V., Gainetdinov, R.R., and Espinoza, S. (2022) Improved cognitive performance in trace amine-associated receptor 5 (TAAR5) knock-out mice. Sci. Rep. *12,* 14708.

53. Aleksandrov, A.A., Polyakova, N.V., Vinogradova, E.P., Gainetdinov, R.R., and Knyazeva, V.M. (2019) The TAAR5 agonist alpha-NETA causes dyskinesia in mice. Neurosci Lett. *704,* 208-211.

54. Kalinina, D.S., Ptukha, M.A., Goriainova, A.V., Merkulyeva, N.S., Kozlova, A.A., Murtazina, R.Z., Shemiakova, T.S., Kuvarzin, S.R., Vaganova, A.N., Volnova, A.B., et al. (2021) Role of the trace amine associated receptor 5 (TAAR5) in the sensorimotor functions. Sci. Rep. *11,* 23092.

55. Romano, K.A., Martinez-Del Campo, A., Kasahara, K., Chittim, C.L., Vivas, E.I., Amador-Noguez, D., Balskus, E.P., and Rey, F.E. (2017) Metabolic, epigenetic, and transgenerational effects of gut bacterial choline consumption. Cell Host Microbe. *22,* 279-290.e7.

56. Mukherji, A., Kobiita, A., Ye, T., and Chambon, P. (2013) Homeostasis in intestinal epithelium is orchestrated by the circadian clock and microbiota cues transduced by TLRs. Cell *153,* 812-827.

57. Asher, G., and Sassone-Corsi, P. (2015) Time for food: the intimate interplay between nutrition, metabolism, and the circadian clock. Cell *161,* 84-92.

58. Thaiss, C.A., Zeevi, D., Levy, M., Zilberman-Schapira, G., Suez, J., Tengeler, A.C., Abramson, L., Katz, M.N., Korem, T., Zmora, N., et al. (2014) Transkingdom control of microbiota diurnal oscillations promote metabolic homeostasis. Cell *159,* 514-529.

59. Liang, X., Bushman, F.D., and FitzGerald, G.A. (2015) Rhythmicity of the intestinal microbiota is regulated by gender and the host circadian clock. Proc. Natl. Acad. Sci. U.S.A. *112,* 10479-10484.

60. Choi, H., Rao, M.C., and Chang, E.B. (2021) Gut microbiota as a transducer of dietary cues to regulate host circadian rhythms in metabolism. Nat. Rev. Gastroenterol. Hepatol. *18,* 679-689.

61. Wang, M., Osborn, L.J., Jain, S., Meng, X., Weakley, A., Yan, J., Massey, W.J., Varadharajan, V., Horak, A., Banerjee, R., et al. (2023) Strain dropout reveal

interactions that govern the metabolic output of the gut microbiome. Cell *186,* 2839-2852.

62. Morales Palomares, S., Parozzi, M., Ferrara, G., Andreoli, D., Godino, L., Gazineo, D., Anastasi, G., Sguanci, M., and Mancin, S. (2025) Olfactory dysfunctions and chronic kidney disease: A scoping review. J. Ren. Nutr. *35,* 4-14.

63. Faour, M., Magnan, C., Gurden, H., and Martin, C. (2022) Olfaction in the context of obesity and diabetes: insights from animal models to humans. Neuropharmacology *206,* 108923.

64. Chen, Y.N., and Kostka, J.K. (2024) Beyond anosmia: olfactory dysfunction as a common denominator in neurodegenerative and neurodevelopmental disorders. *Front Neurosci. 18,* 1502779.

65. Papazian, E.J., and Pinto, J.M. (2021) Olfactory loss and aging: connections with health and well-being. Chem. Senses *46,* bjab045.

66. Chang, K., Zaikos, T., Kilner-Pontone, N., and Ho, C.Y. (2024) Mechanisms of COVID-19-associated olfactory dysfunction. Neuropathol. Appl. Neurobiol. *50,* e12960.

67. Zhu, S., Wang, Y., Li, Y., Li, N., Zheng, Y., Li, Q., Guo, H., Sun, J., Zhai, Q., and Zhu, Y. (2024) TMAO is involved in sleep deprivation-induced cognitive dysfunction through regulating astrocytic cholesterol metabolism via SREBP2. Front. Mol. Neurosci. *17,* 1499591.

68. Giskeødegård, G.F., Davies, S.K., Revell, V.L., Keun, H., and Skene, D.J. (2015) Diurnal rhythms in the human urine metabolome during sleep and total sleep deprivation. Sci. Rep. *5,* 14843.

69. Barrea, L., Muscogiuri, G., Pugliese, G., Graziadio, C., Maisto, M., Pivari, F., Falco, A., Tenore, G.C., Colao, A., and Savastano, S. (2021) Association of the chronotype score with circulating trimethylamine N-oxide (TMAO) concentrations. Nutrients. *13,* 1671.

70. Gisladottir, R.S., Ivarsdottir, E.V., Helgason, A., Jonsson, L., Hannesdottir, N.K., Rutsdottir, G., Arnadottir, G.A., Skuladottir, A., Jonsson, B.A., Norddahl, G.L., et al. (2020) Sequence variants in TAAR5 and other loci affect human odor perception and naming. Curr Biol. *30,* 4643-4653.

71. Moiseenko VI, Apryatina VA, Gainetdinov RR, Apryatin SA. (2024) Trace amine-associated receptors' role in immune system function. Biomedicines *12,* 893.

72. Fergusson, G., Ethier, M., Guévremont, M., Chrétien, C., Attané, C., Joly, E., Fioramonti, X., Prentki, M., Poitout, V., and Alquier, T. (2014) Defective insulin secretory response to intravenous glucose in C57Bl/6J compared to C57Bl/6N mice. Mol. Metab. *3,* 848-854.

73. Attané, C., Peyot, M.L., Lussier, R., Zhang, D., Joly, E., Madiraju, S.R., and Prentki, M. (2016) Differential insulin secretion of high-fat diet-fed C57BL/6NN and C57BL/6NJ

mice: Implications of mixed genetic background in metabolic studies. PLoS One *11,* e0159165.

74. Massey, W., Osborn, L.J., Banerjee, R., Horak, A., Fung, K.K., Orabi, D., Chan, E.R., Sangwan, N., Wang, Z., and Brown, J.M. (2022) Flavin-containing monooxygenase 3 (FMO3) is critical for dioxin-induced reorganization of the gut microbiome and host insulin sensitivity. Metabolites *12,* 364.

75. Bolyen, E., Rideout, J.R., Dillon, M.R., Bokulich, N.A., Abnet, C.C., Al-Ghalith, G.A., Alexander, H., Alm, E.J., Arumugam, M., Asnicar, F., et al. (2019) Reproducible, interactive, scalable and extensible microbiome data science using QIIME 2. Nat Biotechnol. 37, 852-857.

76. Callahan, B.J., McMurdie, P.J., Rosen, M.J., Han, A.W., Johnson, A.J., and Holmes, S.P. (2016) DADA2: high-resolution sample inference from Illumina amplicon data. Nat. Methods 13, 581–583.

77. McMurdie, P.J., and Holmes, S. phyloseq: an R package for reproducible interactive analysis and graphics of microbiome census data. PLoS OneApr 8, e61217.

78. Benjamini, Y., and Hochberg, Y, (1995). Controlling the false discovery rate: A practical and powerful approach to multiple testing, Journal of the Royal Statistical Society, Series B: Methodological *57,* 289–300.

79. Cornelissen, G. (2014) Cosinor-based rhythmometry. Theorectial Biology & Medical Modelling. *11,* 16.

80. Fernandes, A.D., Reid, J.N., Macklaim, J.M., McMurrough, T.A., Edgell, D.R., and Gloor, G.B. (2014) Unifying the analysis of high-throughput sequencing datasets: characterizing RNA-seq, 16S rRNA gene sequencing and selective growth experiments by compositional data analysis. Microbiome *2,* 15.

81. Nelson, W., Tong, Y.L., Lee, J.K., and Halberg, F. (1979) Methods for cosinor-rhythmometry. Chronobiologia *6,* 305-323.

82. Bingham, C., Arbogast, B., Guillaume, G.C., Lee, J.K., and Halberg, F. (1982) Inferential statistical methods for estimating and comparing cosinor parameters. Chronobiologia *9,* 397-439.

83. Lundy, S.D., Sangwan, N., Parekh, N.V., Selvam, M.K.P., Gupta, S., McCaffrey, P., Bessoff, K., Vala, A., Agarwal, A., Sabanegh, E.S., et al. (2021) Functional and Taxonomic Dysbiosis of the Gut, Urine, and Semen Microbiomes in Male Infertility. Eur Urol *79*, 826-836.

HIGHLIGHTS

- Mice lacking the host TMA receptor (*Taar5*$^{-/-)}$ have altered circadian rhythms.
- *Taar5*$^{-/-}$ mice have altered innate behaviors in a time of day dependent manner.
- The normal circadian oscillations in the gut microbiome are dysregulated in *Taar5*$^{-/-}$ mice.
- Genetic deletion of bacterial TMA production or host TMA oxidation shapes circadian rhythms.

ABBREVIATIONS USED

Arntl, basic helix-loop-helix ARNT like 1 or Bmal1; BAT, brown adipose tissue; CKD, chronic kidney disease; *Cry1*, cryptochrome 1; *Cry2*, cryptochrome 2; CVD, cardiovascular disease; EIF2AK3, eukaryotic translation initiation factor 2-alpha kinase 3; ER, endoplasmic reticulum; FMO3, flavin containing monooxygenase 3; GPCR, G protein-coupled receptor; IFNγ, interferon gamma; IL; interleukin; MCP-1, monocyte chemoattractant protein-1; NFκB, nuclear factor κB; NLRP3, nucleotide-binding domain, leucine-rich-containing family, pyrin domain-containing-3; *Nr1d1*, nuclear receptor subfamily 1 group D member 1 or REV-ERBalpha; Pemt, phosphatidylethanolamine *N*-methyltransferase; PERK, eukaryotic translation initiation factor 2-alpha kinase 3; *Per1*, period 1; *Per2*, period 2; *Taar5*, trace amine associated receptor 5; TMA, trimethylamine; TMAO, trimethylamine oxide; WAT, white adipose tissue; ZT, zeitgeber time.

STAR★Methods

Key resources table

REAGENT or RESOURCE	SOURCE	IDENTIFIER
Bacterial and virus strains		
Bacteroides thetaiotaomicron	ATCC	VPI-5482
Bacteroides caccae	ATCC	ATCC 43185
Bacteroides ovatus	ATCC	ATCC 8483
Collinsella aerofaciens	ATCC	ATCC 25986
Eubacterium rectale	ATCC	ATCC 33656
Clostridium sporogenes	ATCC	ATCC 15579
Clostridium sporogenes ΔcutC	Dr. Michael Fischbach at Stanford University	N/A
Chemicals, peptides, and recombinant proteins		
Choline chloride	Sigma	#C7017
Choline chloride (trimethyl-D_9, 98%)	Cambridge Isotope Laboratories, Inc.	#DLM-549-MPT-PK
Betaine	Sigma	#61962
N-(Carboxymethyl)-N,N,N-trimethyl-d9-ammonium Chloride	C/D/N Isotopes Inc.	#D-3352
L-Carnitine hydrochloride	Sigma	#94954
L-Carnitine-d3 HCl (N-methyl-d3)	C/D/N Isotopes Inc.	#D-5069
(3-Carboxypropyl)trimethylammonium chloride (butyrobetaine)	Sigma	#403245
Butyrobetaine-d9	Wang, Z. *et al.*[30]	NA
5-hydroxyindole-3-acetic acid	Sigma	#H8876
5-Hydroxyindole-3-Acetic-2,2-D2 Acid	CDN Isotopes	#D-1547
hippuric acid	Sigma	#8206490100
N-Benzoyl-d5-glycine	CDN Isotopes	#D-5588
4-OH-Hippuric acid	Santa Cruz Biotechnology	#SC-277427
3-hydroxyhippuric acid	TRC	#H943125
2-Hydroxyhippuric Acid	Carbosynth	#FH240191601
Indole-3-Propionic Acid	Alfa Aesar	#L04877
Indole-3-Propionic-2,2-D2 Acid	CDN Isotopes	#D-7686
Methylindole-3-Acetate	Sigma	#I9770
DL-Indole-3-Lactic Acid	Chem-Impex	#21729
Phenylacetic acid	Aldrich	#P16621
Phenylacetic Acid-1,2-13C2	Chem Cruz	#SC-236371
DL-p-Hydrophenyllactic Acid	Aldrich	#H3253
Indoxyl-Glucuronide	Abcam	#Ab146380
L-Tryptophan-2',4',5',6',7'-d5 (indole-d5)	CDN Isotopes	#D-1522
serotonin	Sigma	#H-9523
Tryptamine	Aldrich	#193747
Tryptamine-α,α,β,β-D4 HCl	CDN Isotopes	#D-1546
3-Indoleacetic Acid	Aldrich	#I3750
Indole-3-Acetic-2,2-D2 Acid	CDN Isotopes	#D-1709
Sodium phenyl sulfate	Enamine	#EN300-1704008
TMAO	Sigma	#317594
Trimethylamine *N*-oxide (D_9, 98%)	Cambridge Isotope Laboratories, Inc.	#DLM-4779-1

Phenylacetyl-L-Glutamine	Chem-Impex	#16414
N-alpha-(phenyl-d5-acetyl)-L-glutamine	CDN Isotopes	#D-6900
Potassium p-tolyl sulfate P-cresol sulfate K-salt)	TCI	#P2091
p-Cresol sulfate, potassium salt (D_7, 98%)	Cambridge Isotope Laboratories, Inc.	#DLM-9786
3-Indoxyl Sulfate Potassium Salt	Chem-Impex	#21710
3-Indoxyl Sulfate-d4 Potassium Salt	TRC	#I655102
Phenylacetylglycine	Bachem	#4016439
trans-3-Indoleacrylic acid	Aldrich	#I3807
4-Ethylphenyl sulfate Potassium salt	TRC	#E925865
Trimethylamine hydrochloride	Sigma	#41284
Trimethylamine:DCl (D_{10}, 98%)	Cambridge Isotope Laboratories, Inc.	#DLM-1817-5
Critical commercial assays		
Monarch Total RNA Miniprep Kit	New England BioLabs	#T2010S
V-Plex Cytokine Panel 1 Mouse Kit	Mesoscale Discovery	#K15245D
V-Plex Pro-Inflammatory Panel 1 Mouse Kit	Mesoscale Discovery	#K15048D
U-Plex Metabolic Combo Mouse Kit	Mesoscale Discovery	#K15297K
Ultra Sensitive Mouse Insulin ELISA	Crystal Chem Inc.	#90080
DNeasy PowerSoil Pro Kit	Qiagen	#47014
Experimental models: Organisms/strains		
Germ/free C57BL/6NTac	Taconic	Stock #: B6-GF-F
C57BL/6J	Jackson	#00664
C57BL/6J *Taar5*$^{-/-}$	This paper	NA
C57BL/6J *Fmo3*$^{-/-}$	Massey *et al.*[73]	NA
Oligonucleotides		
LacZ Forward: CCAACGTGACCTATCCCATTAC	Sigma	NA
LacZ Reverse: ATCTTCCTGAGGCCGATACT	Sigma	NA
Arntl1 Forward: CCAAGAAAGTATGGACACAGACAAA	Sigma	NA
Arntl1 Reverse: GCATTCTTGATCCTTCCTTGGT	Sigma	NA
Nr1d1 Forward: ATGCCAATCATGCATCAGGT	Sigma	NA
Nr1d1 Reverse: CCCATTGCTGTTAGGTTGGT	Sigma	NA
Per1 Forward: TGTCCTGGTTTCGAAGTGTG	Sigma	NA
Per1 Reverse: TGTGTCAAGCAGGTTCAGG	Sigma	NA
Per2 Forward: GCTGACGCACACAAAGAACT	Sigma	NA
Per2 Reverse: TAGCCTTCACCTGCTTCACG	Sigma	NA
Clock Forward: AGGCACAGACATTATCGG	Sigma	NA
Clock Reverse: ACCGTCTCATCAAGGGAC	Sigma	NA
Cry1 Forward: TACTGGGAAACGCTGAACCC	Sigma	NA
Cry1 Reverse: ACCCCAAGCTTGTTGCCTAA	Sigma	NA
Cry2 Forward: GCTGGAAGCAGCCGAGGAACC	Sigma	NA
Cry2 Reverse: GGGCTTTGCTCACGGAGCGA	Sigma	NA
Prdm16 Forward: CAGCACGGTGAAGCCATTC	Sigma	NA
Prdm16 Reverse: GCGTGCATCCGCTTGTG	Sigma	NA
Ucp1 Forward: ACTGCCACACCTCCAGTCATT	Sigma	NA
Ucp1 Reverse: CTTTGCCTCACTCAGGATTGG	Sigma	NA
Pemt Forward: TGTGCTGTCCAGCTTCTATG	Sigma	NA
Pemt Reverse: GAAGGGAAATGTGGTCACTCT	Sigma	NA
Pdk4 Forward: GTGCTCTCTGGTCCTCTGTG	Sigma	NA
Pdk4 Reverse: AGTCCAACGGACAAAACGGA	Sigma	NA
Fmo3 Forward: CCCACATGCTTTGAGAGGAG	Sigma	NA

Fmo3 Reverse: GGAAGAGTTGGTGAAGACCG	Sigma	NA
CycloA Forward: GCGGCAGGTCCATCTACG	Sigma	NA
CycloA Reverse: GCCATCCAGCCATTCAGTC	Sigma	NA
Gapdh Forward: CCTCGTCCCGTAGACAAAATG	Sigma	NA
Gapdh Reverse: TGAAGGGGTCGTTGATGGC	Sigma	NA
Software and algorithms		
GraphPad Prism	https://www.graphpad.com/	Version 10.4.1
DADA2	https://benjjneb.github.io/dada2/	Version 3.16
metagenomeSeq	https://github.com/HCBravoLab/metagenomeSeq	Version: Release (3.20)
DAtest	https://github.com/Russel88/DAtest	Version 2.8.0.
ggplot2	https://cran.r-project.org/web/packages/ggplot2/index.html	Version 3.5.1
cosinor	https://cran.r-project.org/web/packages/cosinor/index.html	Version 1.2.3
cosinor2	https://cran.r-project.org/web/packages/cosinor2/index.html	Version 0.2.1
EthoVision XT15 (video tracking software)	Noldus	NA
Other		
qScript	QuantaBio	#95048-100
Fast SYBR Green Master Mix	Applied Biosystems	#4385612
Nutter Butter Cookies	Nabisco	NA
Marbles	Moon Marble Company	NA
SR-LAB-Startle Response System	San Diego Instruments	#2325-0400
Elevated Plus Maze	Nationwide Plastics	NA
Y Maze	Nationwide Plastics	NA
Forepaw Grip Strength Meter	Columbus Instruments	#1027SM
Rotamex-5	Columbus Instruments	#0254–8000
Fear Conditioning Chambers	Med Associates	#VFC-008
Hot Plate	Ugo Basile	#35300
OxyMax Clams Home Cage System	Columbus Instruments	NA

EXPERIMENTAL PROCEDURES

Animal Studies (Mice)

Taar5$^{-/-}$ mice [Taar5$^{tm1.1(KOMP)Vlcg}$] used here were created from ES cell clone 10675A-A8 and originated on the C57BL/6N background by Regeneron Pharmaceuticals, Inc. The successfully

targeted ES cells were then used to create live mice by the KOMP Repository and the Mouse Biology Program at the University of California Davis. It is important to note that this KO/reporter mouse line has the removal of the neomycin selection cassette and critical exon(s) leaving behind the inserted *lacZ* reporter sequence knocked into the *Taar5* locus. Given the well appreciated differences in metabolic homeostasis between C57BL/6N and C57BL/6J substrains[72,73], we backcrossed this line > 10 generations into the C57BL/6J congenic strain and backcrossing was confirmed by mouse genome SNP scanning at the Jackson Laboratory (Bar Harbor, ME). Heterozygous mice on a pure C57BL/6J background were bred to generate littermate *Taar5*$^{+/+}$ and *Taar5*$^{-/-}$ mice. Global *Fmo3*$^{-/-}$ mice on a pure C57BL/6J background have been previously described.[74] All mice were fed standardized control chow diet with defined sufficient level of dietary choline (Envigo diet TD:130104) that was twice irradiated for sterilization. For studies of circadian rhythms, 9-week-old C57Bl6/J male mice were adapted for 2 weeks with a strict 12:12 light:dark cycle. After 7 days, plasma and tissue were collected every 4 hours over a 24-hour period. All dark cycle necropsies were performed under red light conditions to avoid light-driven circadian cues. For the CutC mutant studies shown in main Figure 4, 7-8 week-old germ-free B6/N mice were purchased from Taconic and placed on a sterile chow. Two weeks later, the mice were given an oral gavage of our 6 member community that included *B. caccae, B. ovatus, B. theta, C. aerofaciens, E. rectale,* and either wild-type or mutant *C. sporogenes* suspended in sterile PBS + 20% glycerol as previously described.[55] Gnotobiotic colonized mice were maintained using the Allentown Sentry SPP Cage System (Allentown, NJ) on a 14 hr:10 hr light:dark cycle. Mice were transferred to a room equipped with 12:12 light-dark cycling while still housed on Allentown Transport Carts. After one week of acclimation, plasma and tissue collection were performed every 4 hours over a 24-hour period. All dark cycle necropsies were performed under red light conditions. For all studies plasma was collected by cardiac puncture, and liver, GWAT, BAT and olfactory bulb were collected, flash-

frozen, and stored at –80°C until the time of analysis. All mice were maintained in an Association for the Assessment and Accreditation of Laboratory Animal Care, International-approved animal facility, and all experimental protocols were approved by the Institutional Animal Care and use Committee of the Cleveland Clinic (Approved IACUC protocol numbers 00001941, 00002609, and 0002866).

RNA and Realtime PCR Methods

RNA isolation and quantitative polymerase chain reaction (qPCR) was conducted using methods previously described with minor modifications.[13,33,46] To extract RNA, the Monarch Total RNA MiniPrep Kit (New England BioLabs, Inc.) was employed, and 325 ng of cDNA was utilized for Realtime PCR on a 384-well plate, using Applied Biosystem's Power SYBR Green PC mix in Roche LightCycler 480 I1. The levels of induced mRNAs were standardized by the ΔΔCT method and were normalized to cyclophilin A. The specificity of the primers was verified by analyzing the melting curves of the PCR products. Primer information is available in the Star Methods table.

Quantification of Plasma Metabolites Using Liquid Chromatography Tandem Mass Spectrometry (LC-MS/MS)

Stable isotope dilution high-performance LC-MS/MS was used for quantification of levels of TMAO, TMA, choline, carnitine, and γ-butyrobetaine and all other reported circulating plasma metabolites as previously described performed on a Shimadzu 8050 triple quadrupole mass spectrometer.[13,33,46] A subset of samples were also analyzed on a Thermo Vanquish liquid chromatograph coupled with a Thermo TSQ Quantiva mass spectrometer. 0.2% of formic acid in water (LC-MS grade) was used as mobile phase A and 0.2% formic acid in acetonitrile was used as mobile phase B. The separation was conducted using the following gradient: 0 min, 5% B; 0-2 min, 5% B; 2-8 min, 5%-100%B; 8-16 mins, 100%B; 16-16.5 mins, 5%B; 16.5-25 mins,

5%B. The flow rate was set at 0.2 ml/min. Samples were injected at 2 µl onto a Phenomenex Gemini C18 analytical column (2.0×150 mm, 3 µm). Column temperature was set at 25°C. The acquired data were processed by Thermo Xcalibur 4.3 software to calculate the concentrations. Both methods used multiple reaction monitoring of precursor and characteristic products as we have previously described.[13,33,46]

Plasma Hormone and Cytokine Quantification

Plasma hormones and cytokine levels were quantified using U-PLEX (product # K15297K) and V-PLEX (K15297K) assays per the manufacturer's instructions (Meso Scale Diagnostics, Rockville, Maryland, USA).

Olfactory Cookie Test

To broadly understand olfactory perception, we performed the olfactory cookie test using methods previously described.[46] Briefly, one day prior to testing, food was removed from the home cage. The following day, a clean cage was filled with ~1.5 inches of clean bedding and a small portion of peanut butter cookie (Nutter Butter, Nabisco®) was placed randomly ~1 cm under the bedding. A test mouse was placed into the cage and given 10 minutes to find the hidden cookie. Latency to find the cookie was recorded.

Marble Burying Test

To test for innate/repetitive behavioral alterations, mice underwent a marble burying test. A clean mouse cage was filled with 2.5-3 inches of bedding. 20 black marbles were placed evenly in 5 rows of 4 across the bedding. A test mouse was placed into the cage and was allowed to bury marbles for 30 minutes. After 30 minutes the number of marbles buried was counted. A marble was defined as buried when < 25% of the marble was visible.

Olfactory Discrimination Tests

These tests were performed as described previously[46]. Briefly, a set of non-social odors (almond, banana, corn oil, and water) and two social odors were prepared. Three 6" cotton-tipped applicators containing a single scent were prepared for each of the five odors. Each odor was presented 3 times in a row for 2 min. The cotton applicator was tapped to the wire cage lid on an empty clean home cage so that the cotton tip was hanging just below the wire lid. All trials were video recorded and the amount of time each mouse spent exploring the cotton tip was recorded.

Three-Box Chamber Tests

Preference: 3-chamber social interaction test was performed using a three-chambered box as described previously[46]. This test consisted of three 10-min trials. During the first trial, the mouse was allowed to explore the three-chamber box in which each end-chamber contained an empty cage (upside down pencil holder). This test was used to determine if mice had a clear preference for a chamber.

Social: In the second trial, the three-chamber box contained a novel stimulus mouse under a cage in one of the end-chambers and an inanimate object (ping pong ball) under a cage in the opposite end-chamber. The test mouse was free to choose between a caged inanimate object and a caged, social target.

Novel Object: For the third trial, the test mouse was free to choose between a caged novel social target (novel mouse) versus the same caged mouse in trial 2 (familiar social target). Locations of inanimate targets and social targets were counterbalanced, and mice were placed back into the home cage for very brief intervals between trials. Total duration in chamber and

interaction zone was recorded using video-tracking and automated Noldus EthoVision XT 14 (Leesburg VA).

Social Interaction with Juvenile

Social interaction with a juvenile was performed in a novel empty home cage under dim white light as described previously[46]. Briefly, following a 15-min habituation, a test mouse was placed in a novel empty cage with a juvenile stimulus mouse (BALB/cJ juvenile mouse; 3 weeks of age; Stock #000651 Jackson Labs) and allowed to directly interact for 2 min. Interaction was scored by observing the duration and number of times the test mouse-initiated contact with or sniffed the juvenile mouse. Contact was considered as any part of the boy touching the other mouse. Three days later the same test mouse and juvenile mouse were paired again in a novel clean cage for 2 min and scored in the same manner.

Startle Test

Mice underwent a startle threshold test using methods previously described.[46] Mice were placed inside holding cylinders that sit atop of a piezoelectric accelerometer that detects and transduces animal movement (SR-LAB Startle Response System; SD Instruments; San Diego, CA). Acoustic stimuli were delivered by high-frequency speakers mounted 33 cm above the cylinders. Mouse movements were digitized and stored using computer software supplied by San Diego Instruments. For the startle reactivity test, mice were subjected to eight presentations of six trial types given in pseudorandom order: no stimulus, 80, 90-, 100-, 110-, or 120-dB pulses. The mean startle amplitudes for each condition were calculated. Chambers were calibrated before each set of mice, and sound levels were monitored using a sound meter (Tandy).

Forepaw Grip Strength Test

Grip strength was measured using a digital grip meter (Chatillon Guage with Mesh bar; Columbus Instruments, Columbus, OH) in which a mouse was suspended by its tail and allowed to grab onto a stainless-steel grid bar that is attached to a force transducer. The mouse was gently pulled away from the meter in a horizontal plane. The force applied to the bar immediately before the mouse released its grip was recorded in grams force by the digital sensor. Mice completed 10 trials with an intertrial interval of a least 30 seconds. The mouse's reported grip strength was the average of all 10 trials.

Hotplate Sensitivity Test

For the hotplate sensitivity test, each mouse received a single trial that lasted a maximum of 30 seconds, and the behavioral response was scored live. To assess sensitivity to hot stimuli, a hot plate (Ugo Basile, Italy) was warmed to 52°C and a mouse was placed on the plate and a tall plexiglass cylinder was placed around the mouse to prevent the animal from leaving. A foot pedal was pressed to start the timer on the hotplate. As soon as the mouse showed a response to the stimuli such as jumping or licking their paws, the foot pedal was pressed again to stop the timer and the mouse was removed from the plate. Latency to respond was recorded.

Rotarod

This was a 2-day task in which mice were placed onto a nonrotating rod (3 cm in diameter) that had ridges for a mouse to grip and was divided into 4 sections that allowed 4 mice to be tested at the same time (Rotamex-5; Columbus Instruments; Columbus, OH). Each mouse was subjected to 4 trials per day with an inter-trial interval of at least 30 minutes to prevent its performance from being impaired by fatigue. For each trial, a mouse was placed onto the rod and allowed to balance itself. When mice were balanced on the rod, the rod started rotating and accelerated from 4 to 40 rpm over a 5-minute period. Latency to stay onto the rod was assessed

with the use of an infrared beam just above the rod and was broken once the mouse fell off the rod. Each mouse was subjected to a total of 8 trials over a 2-day period (4 trial/day). Latency to fall (seconds) was recorded.

Nesting

Nesting behavior was performed in a well-lit room by placing a mouse in a novel home cage with a cotton nestlet (5.5 x 5.5 x 0.5 cm) but no bedding. Height and width of the nests were measured at 30, 60, and 90 min.

Fear Conditioning

Fear conditioning (FC) consisted of a training period and a testing period. For the training period, mice were placed in the fear conditioning boxes (Med Associates; Fairfax VT), with a gridded floor, an inside white light and NIR light, and a fixed NIR camera for video recording. Mice were placed inside the chamber for 2 minutes, and then a 30 second, 90 dB acoustic conditioned stimulus (CS; white noise) co- terminated with a 2 second 0.6 mA foot shock (US). Mice received a total of 3 US-CS pairing, with each pairing separated by 1 minute. The mouse remained in the chamber for 30 seconds after the pairings before returning to its home cage. The testing period occurred 24-hrs after the training period ended. The mouse's freezing behavior (motionless except for respirations) was monitored during testing to access memory. Prior to cue FC testing, the inside of the FC chamber was modified using white plastic sheets, interior lighting, and vanilla extract on a paper towel placed in the bedding chamber to make the chamber look and smell differently than the training period. Mice were placed into this modified chamber and allowed to habituate for 3 minutes. Following 3 minutes the same white noise tone used in training was presented to the mouse for 3 minutes. During the tone presentation mouse freezing behavior was recorded. Total percent freezing for cue FC was recorded.

Elevated Plus Maze

The elevated plus maze task was conducted essentially as described previously.[46] Mice were placed in the center of a black, plexiglass elevated plus maze (each arm 33 cm long and 5 cm wide with 25 cm high walls on closed arms) in a dimly lit room for 5 minutes. Automated video tracking software from Noldus Ethovision XT13 (Leesburg VA) was used to track time spent in the open and closed arms, number of open and closed arm entries, and number of explorations of the open arm (defined as placing head and two limbs into open arm without full entry).

Y-Maze

Spontaneous alteration in Y-Maze was assessed as previously described.[46] Briefly, a mouse was placed into one arm of the Y-maze facing the center (14”). Video-tracking was used to record the spontaneous behavior of each mouse for 10 min. Zone (i.e. arm) alteration was later analyzed using Noldus EthoVision XT14, to determine when a mouse entered 3 consecutive different arms of the maze. Spontaneous alteration % was calculated as follows: Alteration % = #spontaneous alterations/ total number of arm entries -2 x 100.

Open Field

The open field was conducted as described previously[46]. Briefly, mice were placed along the edge of an open arena (44 x 44 x 44 cm) and allowed to freely explore for 10 min. Time spent in the center of the arena 15 x 15 cm as well as locomotor activity were measured. Mice were monitored using Noldus EthoVision XT14 (Leesburg VA).

Morris Water Maze

A 48” diameter, white, plastic, circular, heated pool was filled to the depth of 23.5” with 22°C ± 1°C water made opaque with gothic white, nontoxic, liquid tempera paint in a room with prominent extra-maze cues. Mice were placed in one of the four starting locations facing the pool wall and allowed to swim until finding a 15 cm diameter clear platform for 20 s before being removed to the home cage. If mice did not find the platform within 60 s, they were guided to the platform by the experimenter and remained on the platform for 20 s before being removed to the home cage. Latency to reach the platform, distance traveled to reach the platform, swim speed, and time spent in each of four quadrants were obtained using automated video tracking software from Noldus (Ethovision XT13, Leesburg VA). Mice were trained with 4 trials/day with an intertrial interval of 1–1.5 min for 10 consecutive days between 10 am and 3pm. A probe trial (free swim with the submerged platform removed) was performed as the first trial of the day on days 11. Percent time spent in the target quadrant was calculated. Latency to platform, distance to platform, swim speed, and time spent in the target quadrant was analyzed.

Indirect Calorimetry and Metabolic Cage Measurements During Cold Challenge

Cold-induced metabolic responses were quantified using the Oxymax CLAMS system (Columbus Instruments) as previously described.[13] Briefly, weight matched *Taar5*$^{-/-}$ and *Taar5*$^{+/+}$ mice were acclimated to metabolic cages for 48 hours. Thereafter, physical activity, oxygen consumption (VO_2), carbon dioxide production (VCO_2), and respiratory exchange ratio (RER) were continually monitored for 24 hours at thermoneutrality (30°C), 24 hours at room temperature 22°C, and 24 hours in the cold (4°C). Data represent the last 6 a.m. to 6 a.m. period after adequate acclimation.

16S rRNA gene amplicon sequencing and bioinformatics

16S rRNA gene amplicon sequencing and bioinformatics analysis were performed using our published methods using mouse cecum samples.[33] Briefly, raw 16S amplicon sequence and metadata, were *demultiplexed using split_libraries_fastq.*py script implemented *in QIIME2*.[75] Demultiplexed fastq file was split into sample-specific fastq files using split_sequence_file_on_sample_ids.py script from QIIME2. Individual fastq files without non-biological nucleotides were processed using Divisive Amplicon Denoising Algorithm (DADA) pipeline.[76] The output of the dada2 pipeline [feature table of amplicon sequence variants (an ASV table)] was processed for alpha and beta diversity analysis using *phyloseq*[77], and microbiomeSeq (http://www.github.com/umerijaz/microbiomeSeq) packages in R. We analyzed variance (ANOVA) among sample categories while measuring the of α-diversity measures using plot_anova_diversity function in *microbiomeSeq* package. Permutational multivariate analysis of variance (PERMANOVA) with 999 permutations was performed on all principal coordinates obtained during CCA with the *ordination* function of the *microbiomeSeq* package. Pairwise correlation was performed between the microbiome (genera) and metabolomics (metabolites) data was performed using the microbiomeSeq package.

16S Statistical Analysis

Differential abundance analysis was performed using the random-forest algorithm, implemented in the DAtest package (https://github.com/Russel88/DAtest/wiki/usage#typical-workflow). Briefly, differentially abundant methods were compared with False Discovery Rate (FDR), Area Under the (Receiver Operator) Curve (AUC), Empirical power (Power), and False Positive Rate (FPR). Based on the DAtest's benchmarking, we selected lefseq and anova as the methods of choice to perform differential abundance analysis. We assessed the statistical significance ($P < 0.05$) throughout, and whenever necessary, we adjusted *P*-values for multiple comparisons according to the Benjamini and Hochberg method to control False Discovery Rate.[78] Linear

regression (parametric test), and Wilcoxon (Non-parametric) test were performed on genera and ASVs abundances against metadata variables using their base functions in R (version 4.1.2; R Core Team, 2021).

Metagenomic Sequencing to Detect Oscillatory Patterns Occuring in Gnotobiotic Mice Colonized With Defined Synthetic Communities With or Without CutC

Microbial community DNA extraction and sequencing was performed using methods published by our group earlier[83]. Briefly, DNA extraction from cecum was performed using Qiagen's DNeasy PowerSoil Pro kit. To assess sample integrity, an e-gel (electronic agarose gel) was run. The DNA concentration of each sample was then quantified using a Qubit Fluorometer, which measured the values in ng/μL. Using this concentration data, we prepared each sample for Illumina's Nextera XT library preparation kit, targeting a fragment size of 300–500 bp. After library construction, the fragment size distribution of each library was checked using Agilent's TapeStation 4200. The libraries were then re-quantified with the Qubit Fluorometer. Next, the libraries were pooled in a manner that ensured an even distribution of sequencing reads across all samples. The pooled library was quantified again using both a Qubit Fluorometer and qPCR to determine its molarity in nM. Finally, the pooled library was loaded onto the sequencer for sequencing.

Data Analyses for Circadian Rhythmicity (Cosinor Analyses)

A single cosinor analysis was performed as previously described.[79,80] Briefly, a cosinor analysis was performed on each sample using the equation for cosinor fit as follows:

$$Y(t)=M+A\cos(2\theta/\tau+\phi)$$

where M is the MESOR (midline statistic of rhythm, a rhythm adjusted mean), A is the amplitude (a measure of half the extent of the variation within the cycle), Φ is the acrophase (a measure of the time of overall highest value), and τ is the period. The fit of the model was determined by the residuals of the fitted wave. After a single cosinor fit for all samples, linearized parameters were then averaged across all samples allowing for calculation of delineralized parameters for the population mean. A 24 hour period was used for all analysis. Comparison of population MESOR, amplitude, and acrophase was performed as previously described.[33] Comparisons are based on F-ratios with degrees of freedom representing the number of populations and total number of subjects. All analyses were done in R v.4.0.2 using the cosinor and cosinor2 packages.[80-82]

Standard Statistical Analyses

Data are expressed as the mean ± standard error of the mean (SEM). All data were analyzed using either one-way or two-way analysis of variance followed by Student's t tests for post hoc analysis. Differences were considered significant at $p < 0.05$. All analyses were performed using GraphPad Prism software (version 10.2.2; GraphPad Software, Inc).

Figure Legends

Figure 1. The Host Trimethylamine Receptor TAAR5 Shapes Tissue-Specific Circadian Oscillations. Male chow-fed wild-type (*Taar5*$^{+/+}$) or mice lacking the TMA receptor (*Taar5*$^{-/-}$) were necropsied at 4-hour intervals to collect tissues including skeletal muscle **(A)**, olfactory bulb **(B)**, liver **(C)**, or gonadal white adipose tissue **(D)**. The relative gene expression for circadian (*Arntl, Clock, Nr1d1, Cry1, and Per2*) and metabolism (*Prdm16 and Ucp1*) related genes was quantified by qPCR using the ΔΔ-CT method. Data shown represent the means -/+ S.D. for n= 3-6 individual mice per group. Group differences were determined using cosinor analyses *p*-values are provided where there were statistically significant differences between *Taar5*$^{+/+}$ and *Taar5*$^{-/-}$ mice. The complete cosinor statistical analysis for circadian data can be found in Table 1. * = Significant differences between *Taar5*$^{+/+}$ and *Taar5*$^{-/-}$ mice by student's t-tests within each ZT time point (p<0.05).

Figure 1, figure supplement 1. Body Weights Across a 24-Hour Period in Chow-Fed Male *Taar5*$^{+/+}$ and *Taar5*$^{-/-}$ Mice. Male chow-fed wild-type (*Taar5*$^{+/+}$) or mice lacking the TMA receptor (*Taar5*$^{-/-}$) were necropsied at 4-hour intervals and body weight at necropsy was quantified. Data shown represent the means -/+ S.D. for n= 3-6 individual mice per group. Group differences were tested using cosinor analyses, but no statistically-signficant differences were detected.

Figure 1 – figure supplement 2. The Host Trimethylamine Receptor TAAR5 Shapes Circadian Oscillations in Circulating Hormones and Cytokines. Male chow-fed wild-type mice (*Taar5*$^{+/+}$) or mice lacking the TMA receptor (*Taar5*$^{-/-}$) were necropsied at 4-hour intervals to collect plasma. **(A)** Plasma levels of metabolites in the metaorganismal trimethylamine N-oxide (TMAO) pathway were quantified using liquid chromatography tandem mass spectrometry

(LC-MS/MS). **(B)** Plasma metabolic hormones (insulin, C-peptide, glucagon, GLP-1, leptin, ghrelin, and peptide YY) and cytokine/chemokine (MCP-1, IL-6, and TNFα) levels were quantified using MesoScale Discovery multi-plex immunoassays as described in the materials and methods. Data shown represent the means -/+ S.D. for n= 3-6 individual mice per group. Group differences were determined using cosinor analyses *p*-values are provided where there were statistically significant differences between *Taar5*$^{+/+}$ and *Taar5*$^{-/-}$ mice. The complete cosinor statistical analysis for circadian data can be found in Table 1. Significant differences between Taar5$^{+/+}$ andTaar5$^{-/-}$ mice by student's t-tests within each ZT time point (**p*< 0.05: ***p*< 0.01; ****p* <0.001, and *****p*<0.0005)

Figure 2. Mice Lacking the Host TMA Receptor TAAR5 Have Altered Olfactory and Repetitive Behaviors Only at Specific Circadian Timepoints. Male or female wild-type mice (*Taar5*$^{+/+}$) or mice lacking the TMA receptor (*Taar5*$^{-/-}$) were subjected to the olfactory cookie test **(A)** or the marble burying test **(B)**. To examine circadian alterations in behavior, these tests were done in either the dark-light phase transition (ZT23-ZT1), mid light cycle (ZT5-ZT7), or early dark cycle (ZT13-ZT15). Data represent the mean -/+ S.E.M. from n=10-15 per group when male and female are separated (n=25-27 when both sexes are combined), and statistically significant difference between *Taar5*$^{+/+}$ and *Taar5*$^{-/-}$ mice are denoted by * = p<0.05 and ** = p<0.01.

Figure 2 – figure supplement 1. Olfactory Discrimination of Several Odor Stimuli is Unaltered in *Taar5*-Deficient Mice. Male or female wild-type mice (*Taar5*$^{+/+}$) or mice lacking the TMA receptor (*Taar5*$^{-/-}$) were subjected to a battery of single stimulus olfactory discrimination tests to determine time to and time at each stimuli including: **(A)** banana, **(B)** corn oil, **(C)** almond, **(D)** water, **(E)** or social odors as described in the methods section. Data are shown for the entire cohort combining both sexes or divided into either male or female cohorts to examine sexual

dimorphism in phenotype. Data represent the mean -/+ S.E.M. from n=10-15 per group when male and female are separated (n=25-27 when both sexes are combined). No statistically significant alterations were found during this battery of tests.

Figure 2 – figure supplement 2. *Taar5*-Deficient Mice Exhibit Specific Alterations in Social Behaviors. Male or female wild-type mice (*Taar5*$^{+/+}$) or mice lacking the TMA receptor (*Taar5*$^{-/}$) were subjected to a battery of social behavioral tests including: **(A)** three-chamber preference test, **(B)** three-chamber social preference test, **(C)** three-chamber social novelty test, or **(D)** social interaction with a juvenile as described in the methods section. Data are shown for the entire cohort combining both sexes or divided into either male or female cohorts to examine sexual dimorphism in phenotype. Data represent the mean -/+ S.E.M. from n=10-15 per group when male and female are separated (n=25-27 when both sexes are combined), Significant differences between *Taar5*$^{+/+}$ and *Taar5*$^{-/-}$ mice were determined by student's t-tests (**p*< 0.05: ***p*< 0.01; ****p* <0.001, and *****p*<0.0005)

Figure 2 – figure supplement 3. *Taar5*-Deficient Mice Exhibit Specific Alterations in Innate Behavioral Responses. Male or female wild-type mice (*Taar5*$^{+/+}$) or mice lacking the TMA receptor (*Taar5*$^{-/}$) were subjected to a battery of innate behavioral tests including: **(A)** startle test, **(B)** forepaw grip strength, **(C)** hotplate sensitivity, **(D)** rotorod, and **(E)** nesting as described in the methods section. Data are shown for the entire cohort combining both sexes or divided into either male or female cohorts to examine sexual dimorphism in phenotype. Data represent the mean -/+ S.E.M. from n=10-15 per group when male and female are separated (n=25-27 when both sexes are combined). Significant differences between *Taar5*$^{+/+}$ and *Taar5*$^{-/-}$ mice were determined by student's t-tests (**p*< 0.05: ***p*< 0.01; and ****p* <0.001).

Figure 2 – figure supplement 4. Impact of *Taar5*-Deficiency on Cognitive, Depression, and Anxiety-Like Behaviors. Male or female wild-type mice (*Taar5*$^{+/+}$) or mice lacking the TMA receptor (*Taar5*$^{-/}$) were subjected to a battery of behavioral tests related to cognition, depression, and anxiety including: **(A)** cued fear conditioning, **(B)** elevated plus maze, **(C)** Y-maze, and **(D)** open field tes as described in the methods section. Data are shown for the entire cohort combining both sexes or divided into either male or female cohorts to examine sexual dimorphism in phenotype. Data represent the mean -/+ S.E.M. from n=9-10 per group when male and female are separated (n=19-20 when both sexes are combined). Significant differences between *Taar5*$^{+/+}$ and *Taar5*$^{-/-}$ mice were determined by student's t-tests (**p*< 0.05)

Figure 2 – figure supplement 5. Impact of *Taar5*-Deficiency on Morris Water Maze Performance. Male or female wild-type mice (*Taar5*$^{+/+}$) or mice lacking the TMA receptor (*Taar5*$^{-/}$) were subjected to the Morris water maze as described in the methods section. Data are shown for the entire cohort combining both sexes or divided into either male or female cohorts to examine sexual dimorphism in phenotype. Data represent the mean -/+ S.E.M. from n=10-15 per group when male and female are separated (n=25-27 when both sexes are combined), Significant differences between *Taar5*$^{+/+}$ and *Taar5*$^{-/-}$ mice were determined by student's t-tests (**p*< 0.05: ***p*< 0.01; ****p* <0.001, and *****p*<0.0005)

Figure 2 – figure supplement 6. Impact of *Taar5*-Deficiency on Systemic Energy Metabolism and Gene Expression in Brown Adipose Tissue (BAT). (A) Male or female wild-type mice (*Taar5*$^{+/+}$) or mice lacking the TMA receptor (*Taar5*$^{-/}$) were place in individual cages for indirect calorimetry measured using the Oxymax CLAMS home cage system. After two days of equillbration, mice were maintained at thermoneutrality (30°C), room temperature (22°C), or cold stressed (4°C) over a 24-hour period at each temperature point. Oxygen consumption was

quantified throughout these temperature transitions as described in the methods section. **(B)** Male or female wild-type mice (*Taar5*$^{+/+}$) or mice lacking the TMA receptor (*Taar5*$^{-/}$) were necropsied at the beginning of the light cycle (ZT2) or the beginning of the dark cycle (ZT14) and subscapular brown adipose tissue (BAT) was harvested to examine gene. The relative gene expression for circadian genes (*Arntl, Nr1d1, Cry1, and Per1*) was quantified by qPCR using the ΔΔ-CT method. Data represent the mean -/+ S.E.M. from n=5-9 per group. Significant differences between *Taar5*$^{+/+}$ and *Taar5*$^{-/-}$ mice were determined by student's t-tests within each individual time point (*p< 0.05)

Figure 3. The Trimethylamine Receptor TAAR5 Shapes Circadian Oscillations in the Gut Microbiome. Male chow-fed wild-type (*Taar5*$^{+/+}$) or mice lacking the TMA receptor (*Taar5*$^{-/-}$) were necropsied at 4-hour intervals to collect cecum for microbiome composition analyses via sequencing the V4 region of the 16S rRNA (genus level changes are shown). **(A)** Canonical correspondence analysis (CCA) based beta diversity analyses show distinct microbiome compositions in *Taar5*$^{+/+}$ and *Taar5*$^{-/-}$ mice. Statistical significance and beta dispersion were estimated using PERMANOVA. **(B)** The relative abundance of cecal microbiota in *Taar5*$^{+/+}$ and *Taar5*$^{-/-}$ mice. Significantly altered cecal microbial genera in *Taar5*$^{+/+}$ and *Taar5*$^{-/-}$ mice are shown at ZT2 **(C)**, ZT6 **(D)**, ZT10 **(E)**, ZT14 **(F)**, ZT18 **(G)**, and ZT22 **(H)**. ASVs that were significantly different in abundance (MetagenomeSeq with Benjamini-Hochberg FDR multiple test correction, adjusted p<0.01). Data shown represent the means -/+ S.D. for n= 3-6 individual mice per group. Group differences were determined using ANOVA with Benjamini-Hochberg false discovery rate (FDR) multiple test correction, * = adjusted p<0.01.

Figure 3 – figure supplement 1. TAAR5-Deficient Mice Have Altered Circadian Oscillations in the Gut Microbiome at the Phylum Level. Male chow-fed wild-type (*Taar5*$^{+/+}$) or mice

lacking the TMA receptor (*Taar5*$^{-/-}$) were necropsied at 4-hour intervals to collect cecum for microbiome composition analyses via sequencing the V4 region of the 16S rRNA (phylum level changes are shown). Data shown represent the means -/+ S.D. for n= 3-6 individual mice per group. The relative abundance of cecal microbiota at the phylum level are shown, and group differences were determined using cosinor analyses *p*-values are provided where there were statistically significant differences between *Taar5*$^{+/+}$ and *Taar5*$^{-/-}$ mice.

Figure 3 – figure supplement 2. TAAR5-Deficient Mice Have Altered Circadian Oscillations in the Gut Microbiome. Male chow-fed wild-type (*Taar5*$^{+/+}$) or mice lacking the TMA receptor (*Taar5*$^{-/-}$) were necropsied at 4-hour intervals to collect cecum for microbiome composition analyses via sequencing the V4 region of the 16S rRNA (genus level changes are shown). The relative abundance of cecal microbiota at the genus level are shown, and group differences were determined using cosinor analyses *p*-values are provided where there were statistically significant differences between *Taar5*$^{+/+}$ and *Taar5*$^{-/-}$ mice. Data shown represent the means -/+ S.D. for n= 3-6 individual mice per group. Group differences were tested using cosinor analyses (key statistics represented here), and the complete cosinor statistical analysis for circadian data can be found in Table 1. * = Significant differences are also shown between *Taar5*$^{+/+}$ and *Taar5*$^{-/-}$ mice by student's t-tests within each ZT time point ($p<0.05$).

Figure 4. Transplanting a Defined Synthetic Microbial Community With or Without Genetically Deleted Trimethylamine Production Capacity (*ΔcutC*) Alters Host Circadian Rhythms. Germ-free C57Bl/6 mice (recipients) were gavaged with the core community (*B. caccae, B. ovatus, B. thetaiotaomicron, C. aerofaciens, E. rectale*) with TMA producing wild-type (WT) *C. sporogenes* (produces TMAO) or *C. sporogenes* Δ*cutC.* Gnotobiotic mice were then necropsied at 4-hour intervals to collect tissues including plasma (**A** and **C**) and olfactory bulb

(B). (A) Plasma levels of TMAO pathway metabolites (choline, L-carnitine, betaine, γ-butyrobetaine, trimethylamine (TMA), and trimethylamine N-oxide (TMAO)) were quantified by liquid chromatography tandem mass spectrometry (LC-MS/MS). (**B**) PCR was performed on olfactory bulb to examine key circadian clock regulators. **(C)** Plasma levels of metabolic hormones (insulin, GLP-1, and leptin) and select cytokines including interleukins (IL-1β, IL-2, and IL-33) were measured as described in the methods section. Data shown represent the means -/+ S.E.M. for n= 5-6 individual mice per group. Differences between WT-*cutC* and Δ*cutC* groups were determined using cosinor analyses *p*-values are provided where there were statistically significant differences between group for circadian statistics. The complete cosinor statistical analysis for circadian data can be found in Table 1. Significant differences between WT-*cutC* and Δ*cutC* groups were also analyzed by student's t-tests within each ZT time point (* = $p<0.05$ and ** = $p<0.01$).

Figure 4, figure supplement 1. The Oscillatory Patterns of the TMAO-Defined Community is Altered When cutC is Genetically Deleted. Germ-free C57Bl/6 mice (recipients) were gavaged with the core community (*B. caccae, B. ovatus, B. thetaiotaomicron, C. aerofaciens, E. rectale*) with TMA producing wild-type (WT) *C. sporogenes* (produces TMAO) or *C. sporogenes* Δ*cutC.* Gnotobiotic mice were then necropsied at 4-hour intervals to collect cecum for shotgun metagenomic sequencing. The total abundance is shown for each of the five bacteria represented in the defined community over the 24-hour circadian period. Differences between WT-*cutC* and Δ*cutC* groups were determined using cosinor analyses *p*-values are provided where there were statistically significant differences between group for circadian statistics. The complete cosinor statistical analysis for circadian data can be found in Table 1. Significant differences between WT-*cutC* and Δ*cutC* groups were also analyzed by student's t-tests within each ZT time point (* = $p<0.05$ and ** = $p<0.01$).

Figure 4 – figure supplement 2. Mice Lacking Either Gut Microbial TMA Production or Host-Driven TMA Oxidation Have Altered Circadian Rhythms. (A,B) Female germ-free C57Bl/6 mice (recipients) were gavaged with the core community (*B. caccae, B. ovatus, B. thetaiotaomicron, C. aerofaciens, E. rectale*) with TMA producing wild-type (WT) *C. sporogenes* (produces TMAO) or *C. sporogenes* Δ*cutC.* Gnotobiotic mice were then necropsied at 4-hour intervals to collect tissues including subscapular brown adipose tissue **(A)** and plasma **(B).** Gene expression was quantified by qPCR and metabolite levels were quantified by LC-MS/MS as described in the method section. Data for panels A and B were analyzed by cosinor analyses and representative p-values are shown; The complete statistical analysis for cosinor circadian metrics can be found in Table 1. **(C)** Female wild-type (*Fmo3*$^{+/+}$) or flavin-containing monooxygenase 3 knockout (*Fmo3*$^{-/-}$) mice were necropsied at ZT2 or ZT14 and TMAO levels were measured by LC-MS/MS and olfactory bulb circadian gene expression was quantified by qPCR. Data shown represent the means -/+ S.E.M. for n= 4-6 individual mice per group. Significant differences between by student's t-tests within each ZT time point (* = $p<0.05$ and ** = $p<0.01$).

Main Figure 1

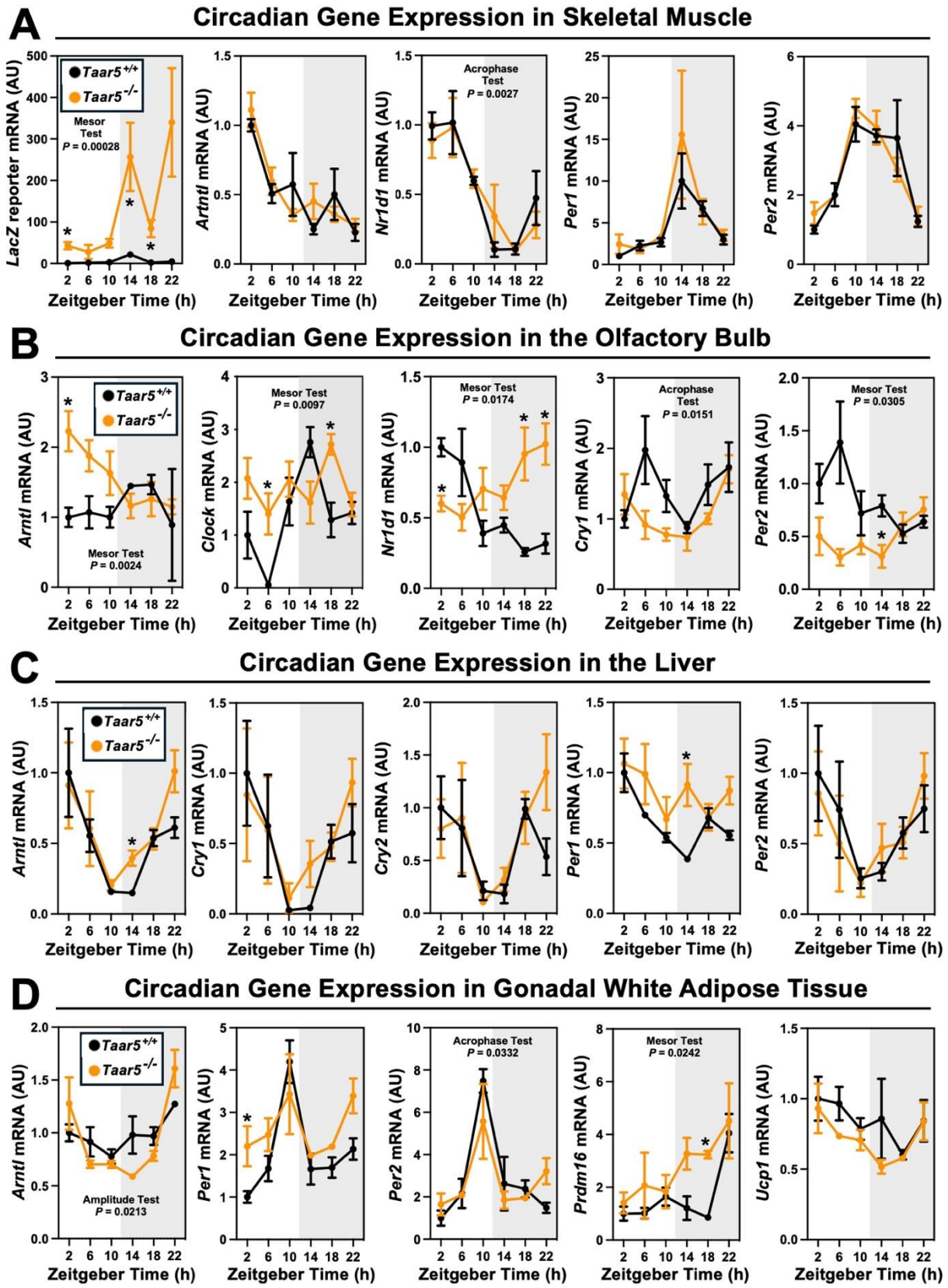

Figure 1 – figure supplement 1

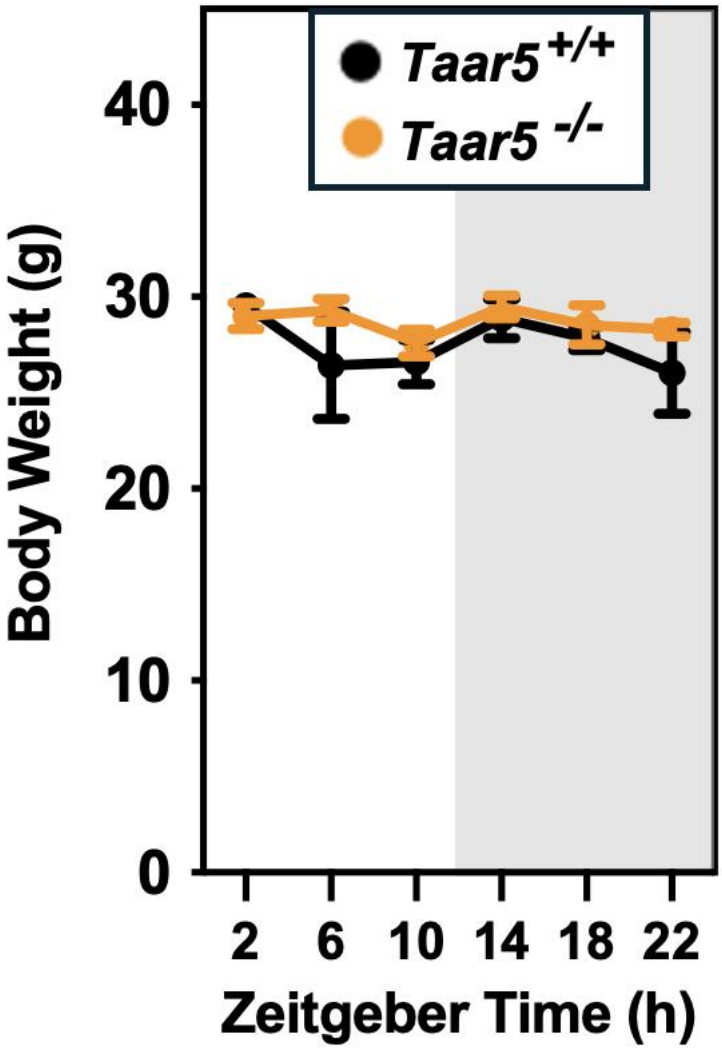

Figure 1 – figure supplement 2

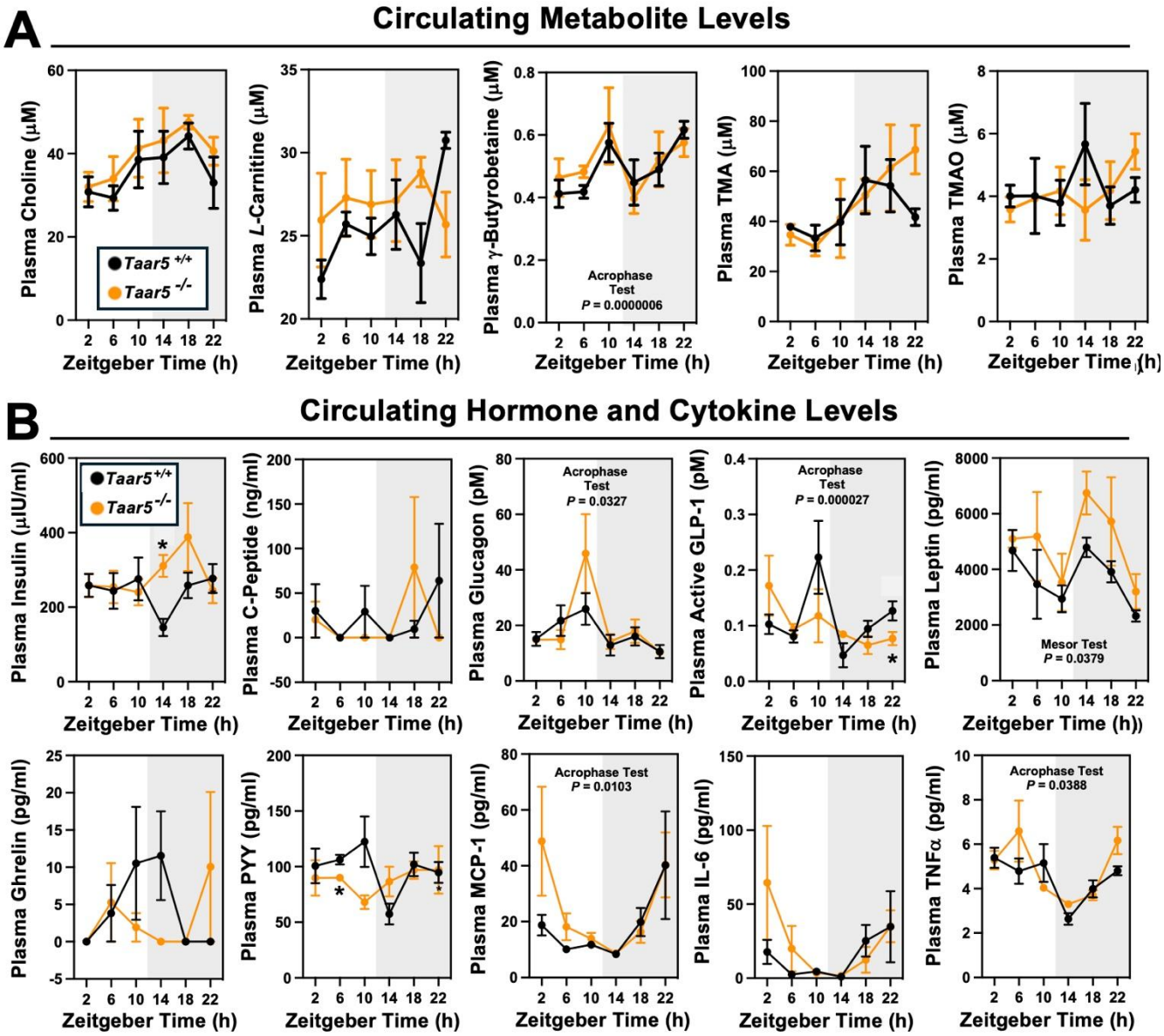

Main Figure 2

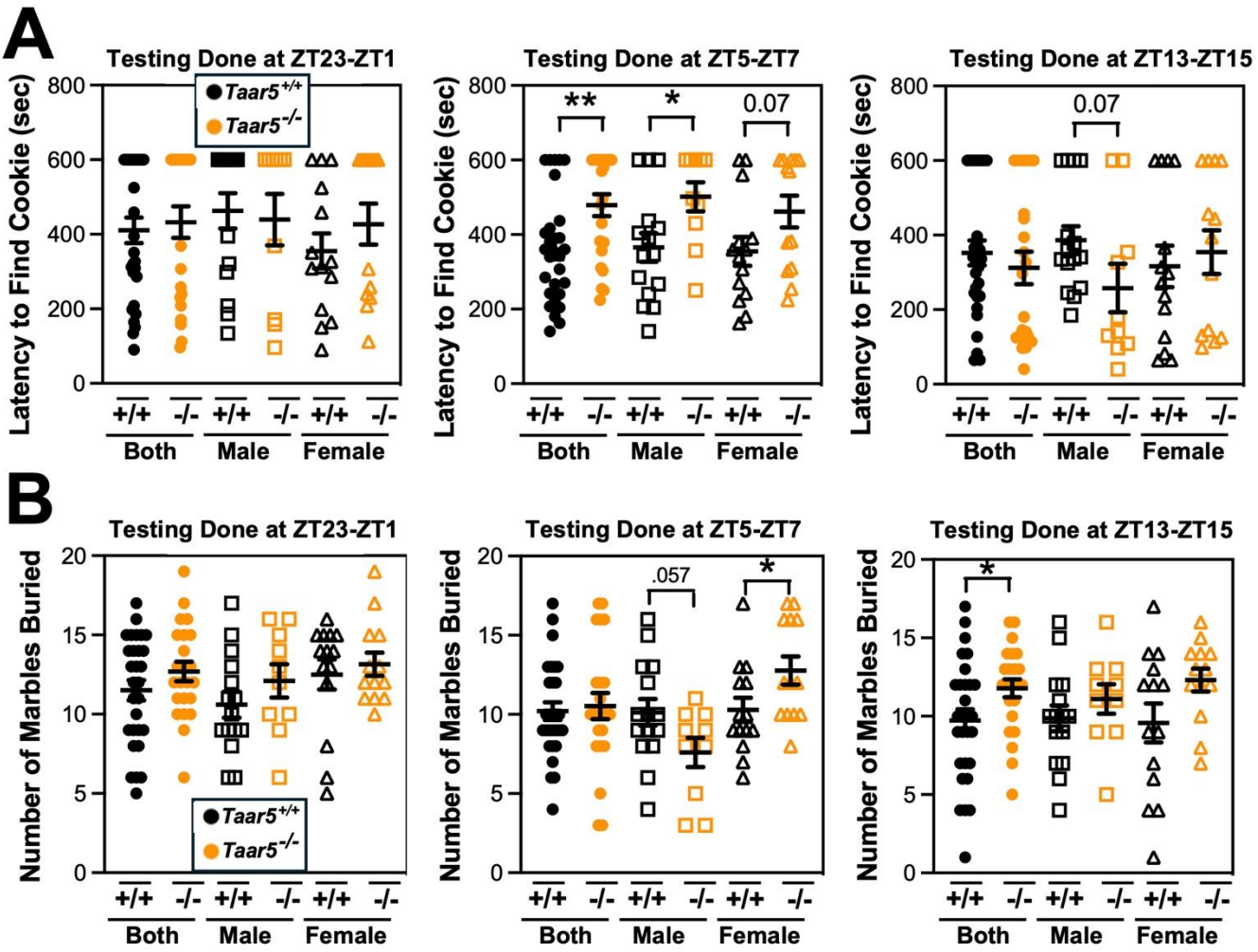

Figure 2 – figure supplement 1

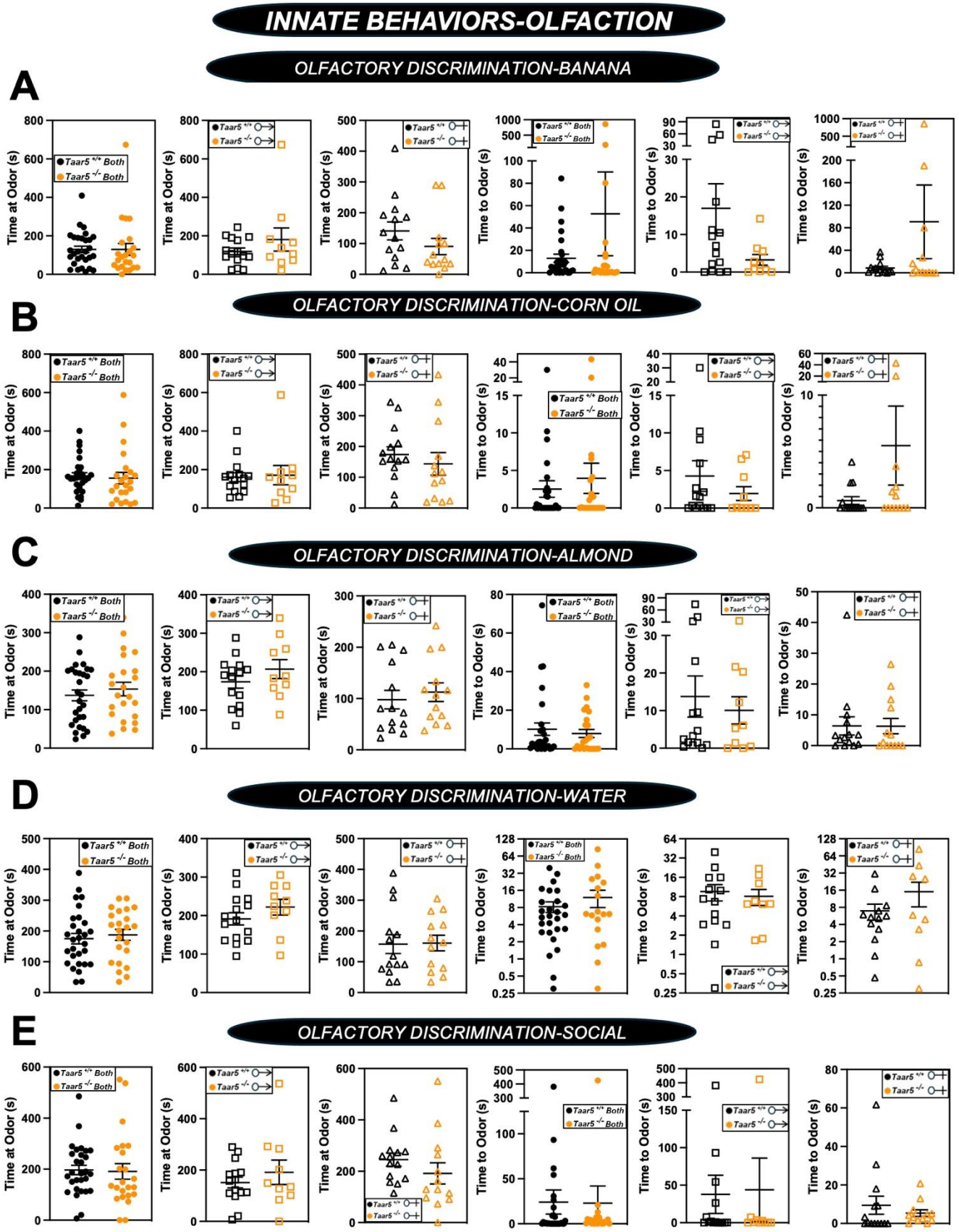

Figure 2 – figure supplement 2

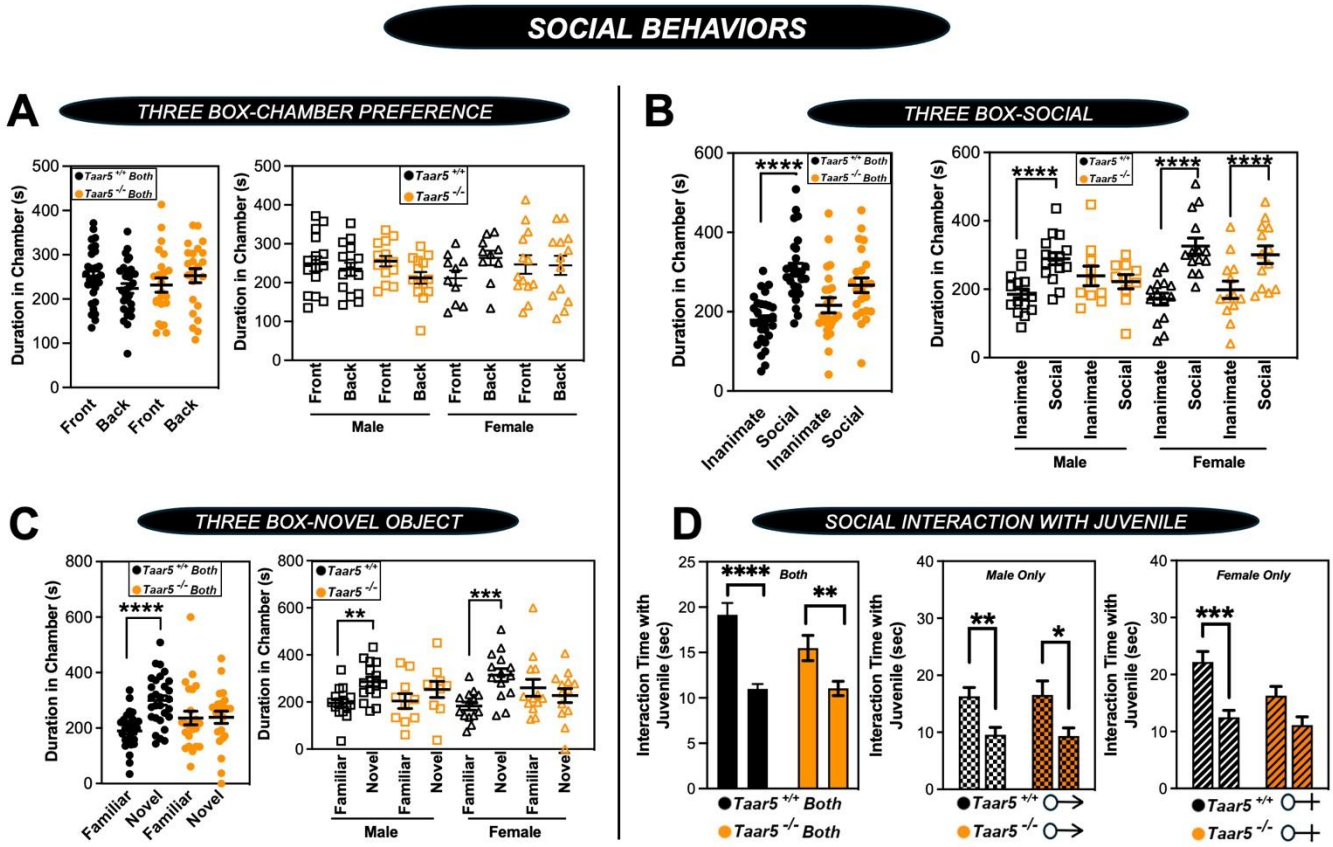

Figure 2 – figure supplement 3

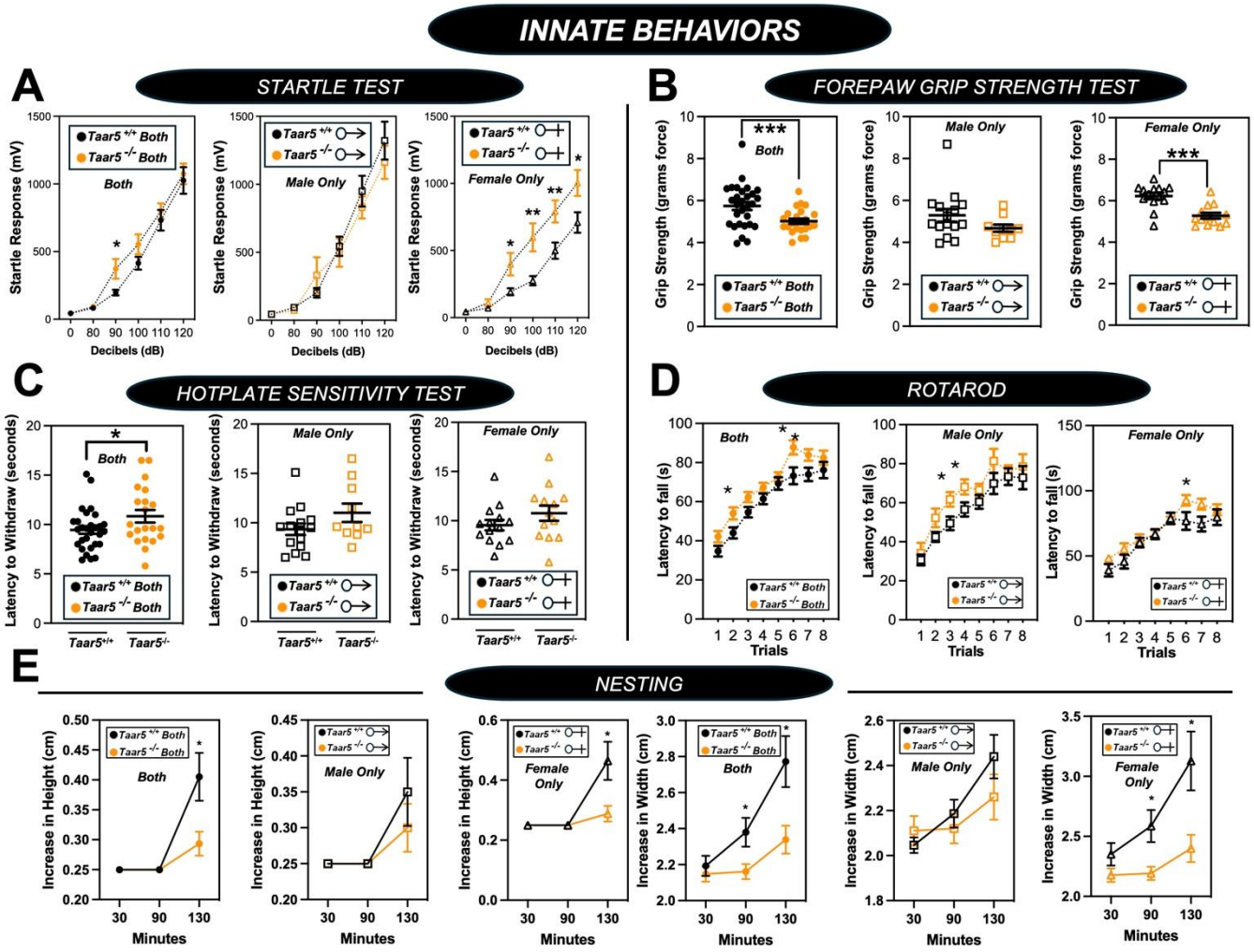

Figure 2 – figure supplement 4

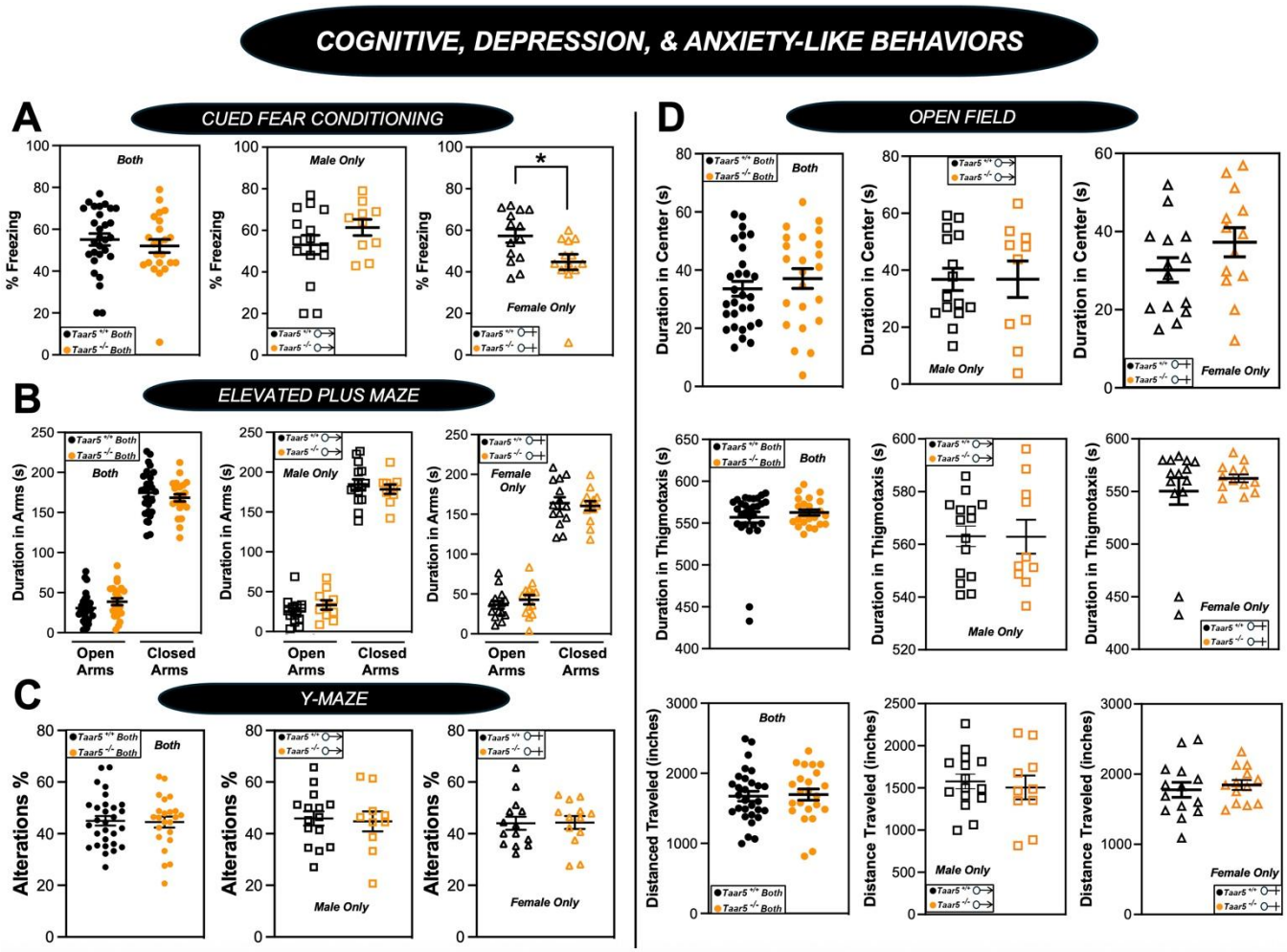

Figure 2 – figure supplement 5

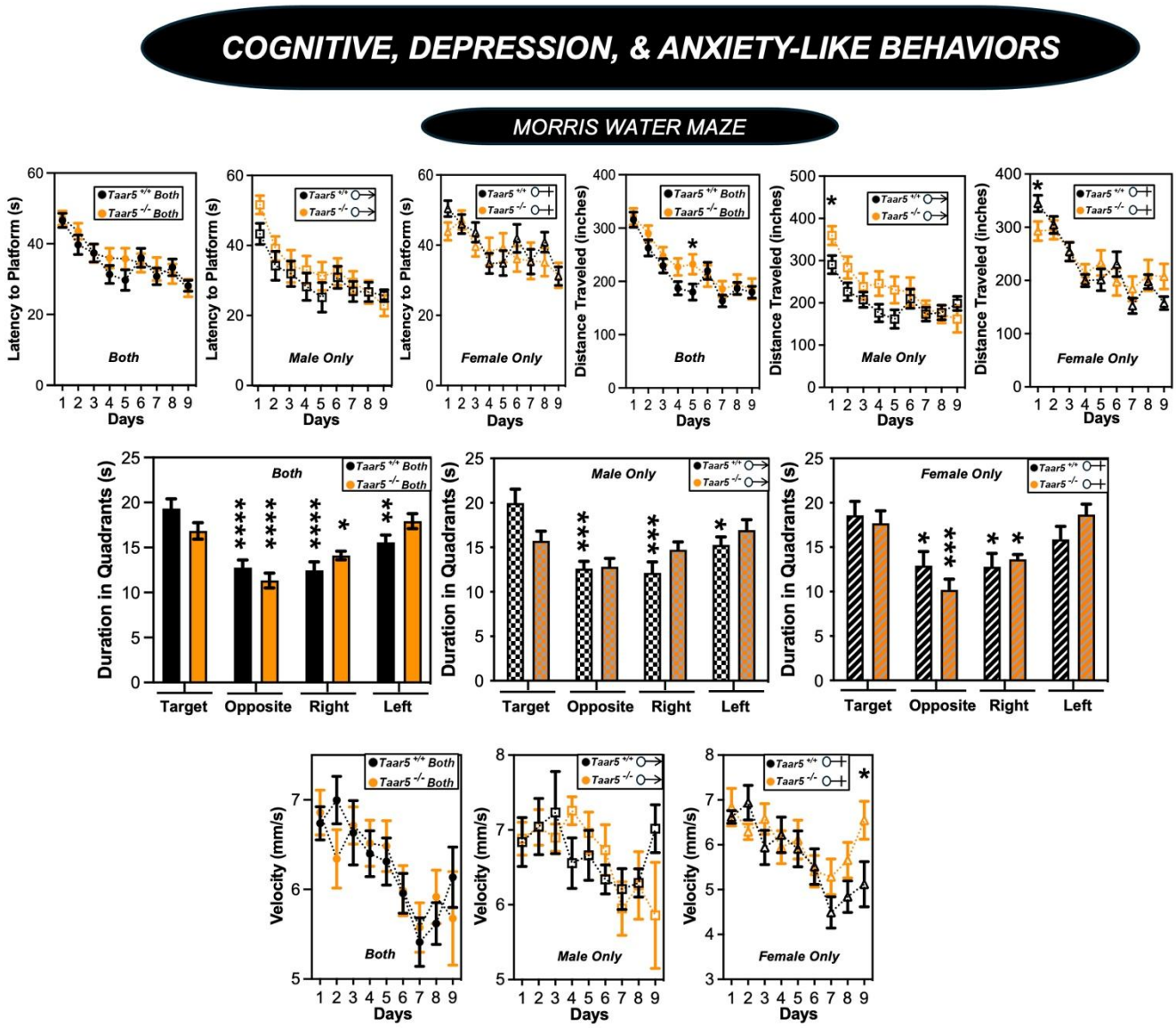

Figure 2 – figure supplement 6

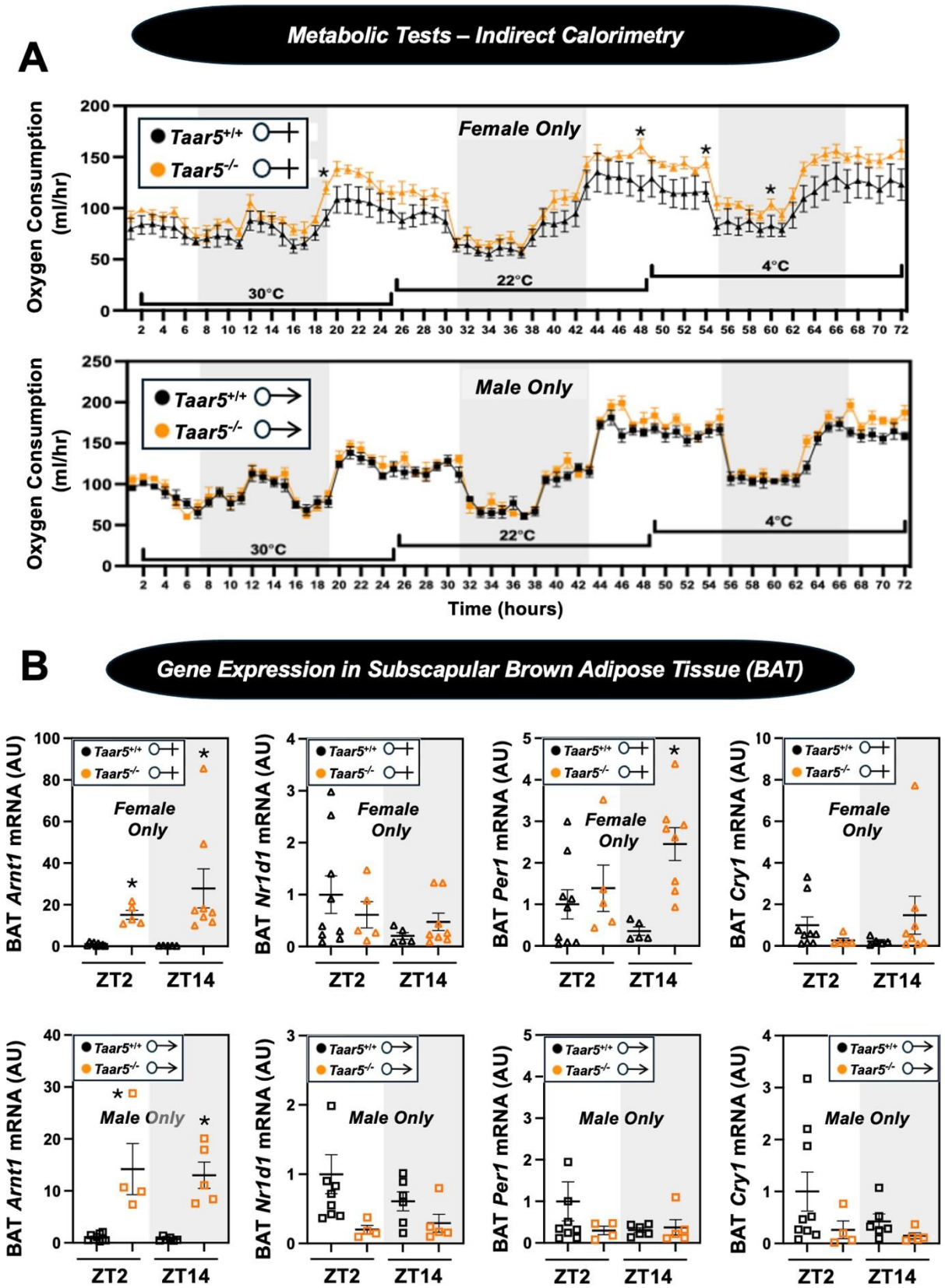

Main Figure 3

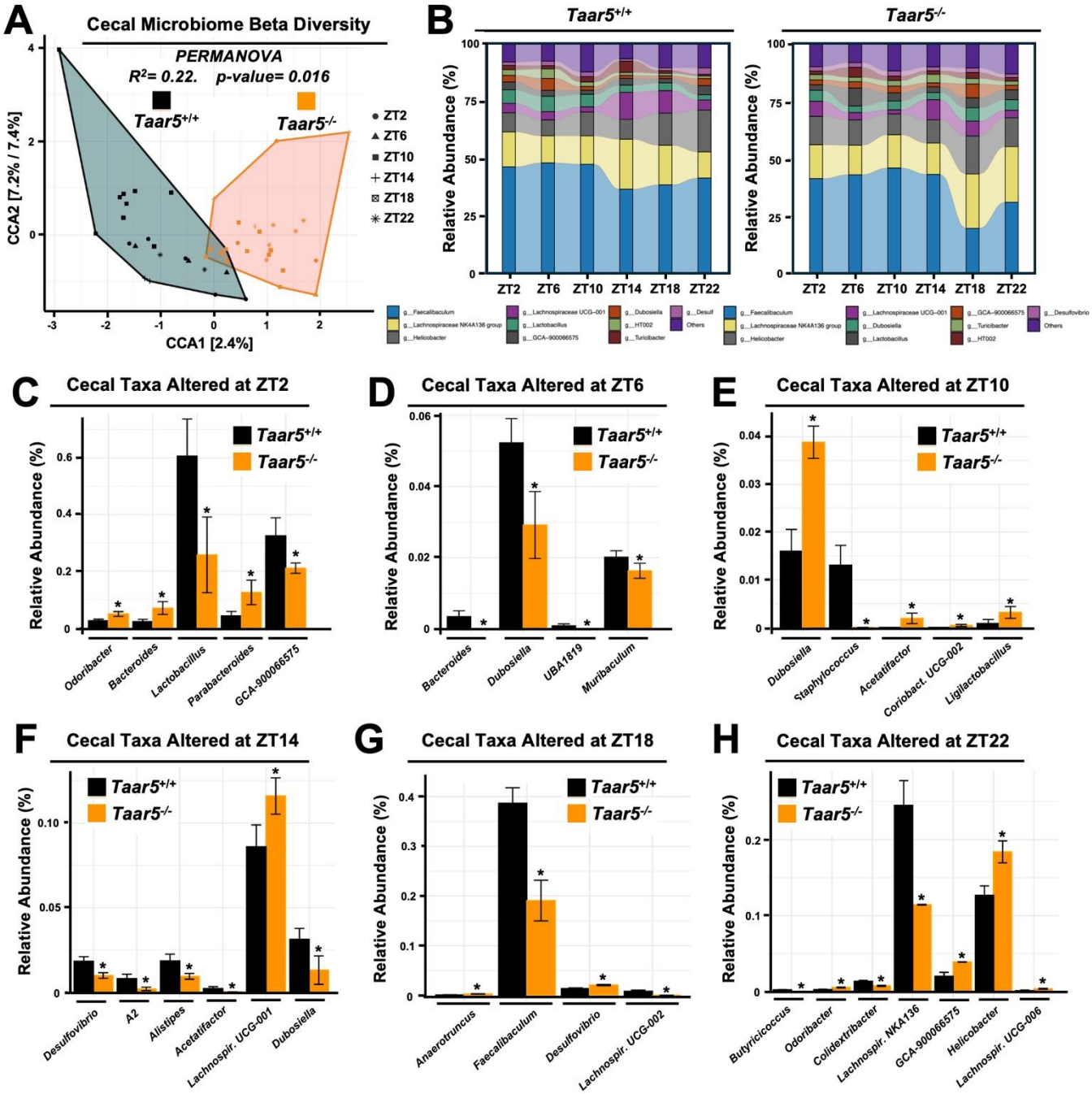

Figure 3 – figure supplement 1

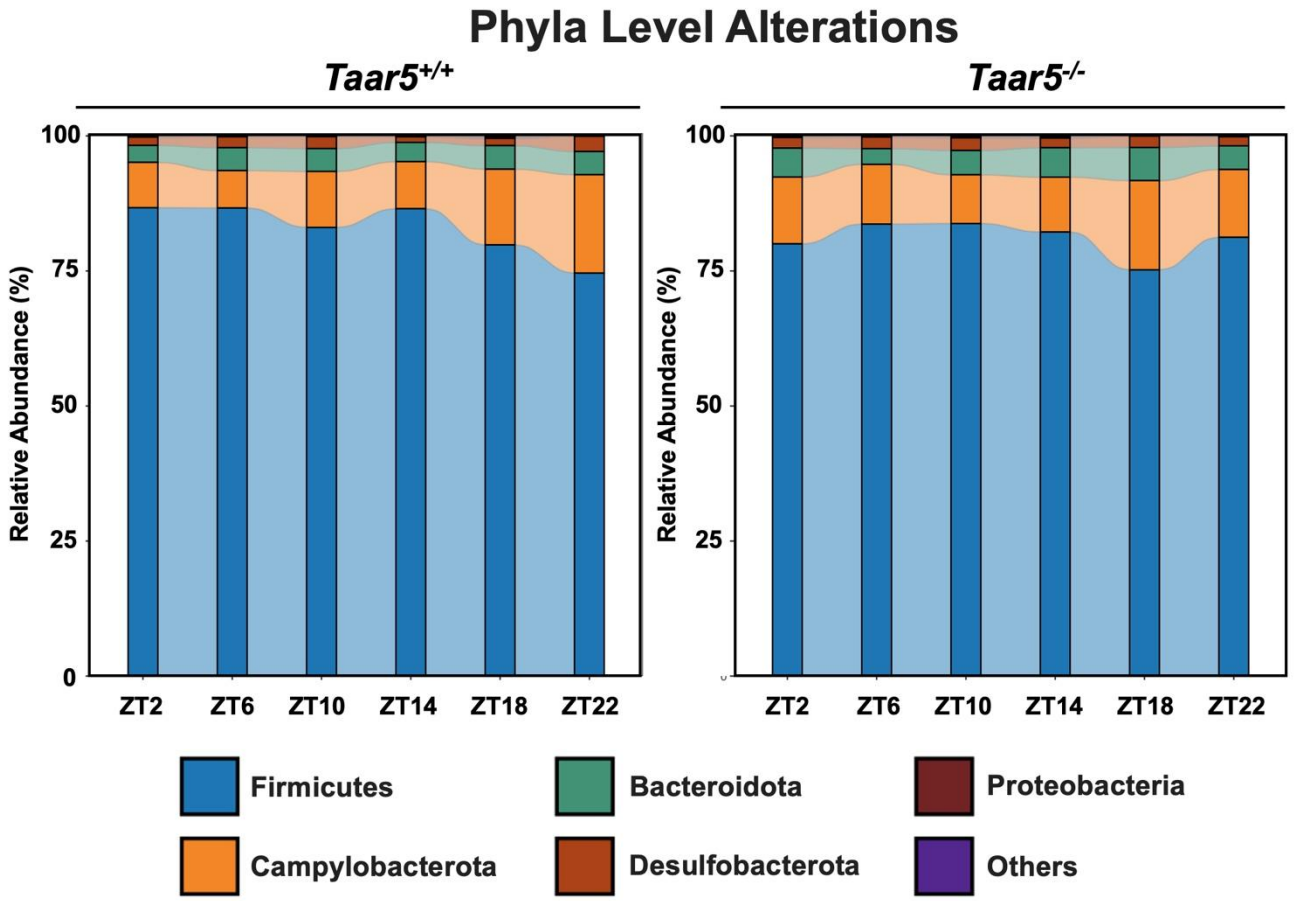

Figure 3 – figure supplement 2

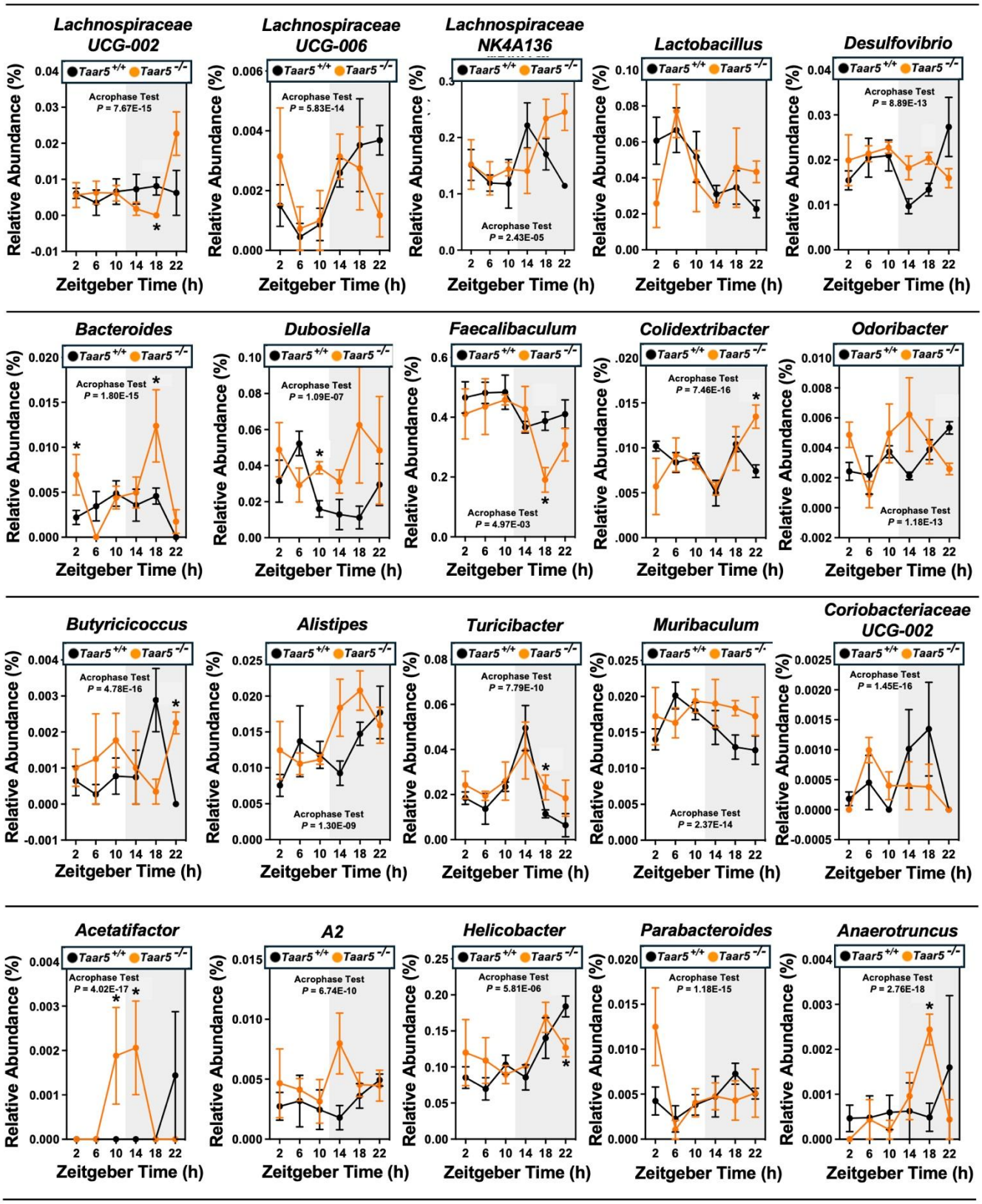

Main Figure 4

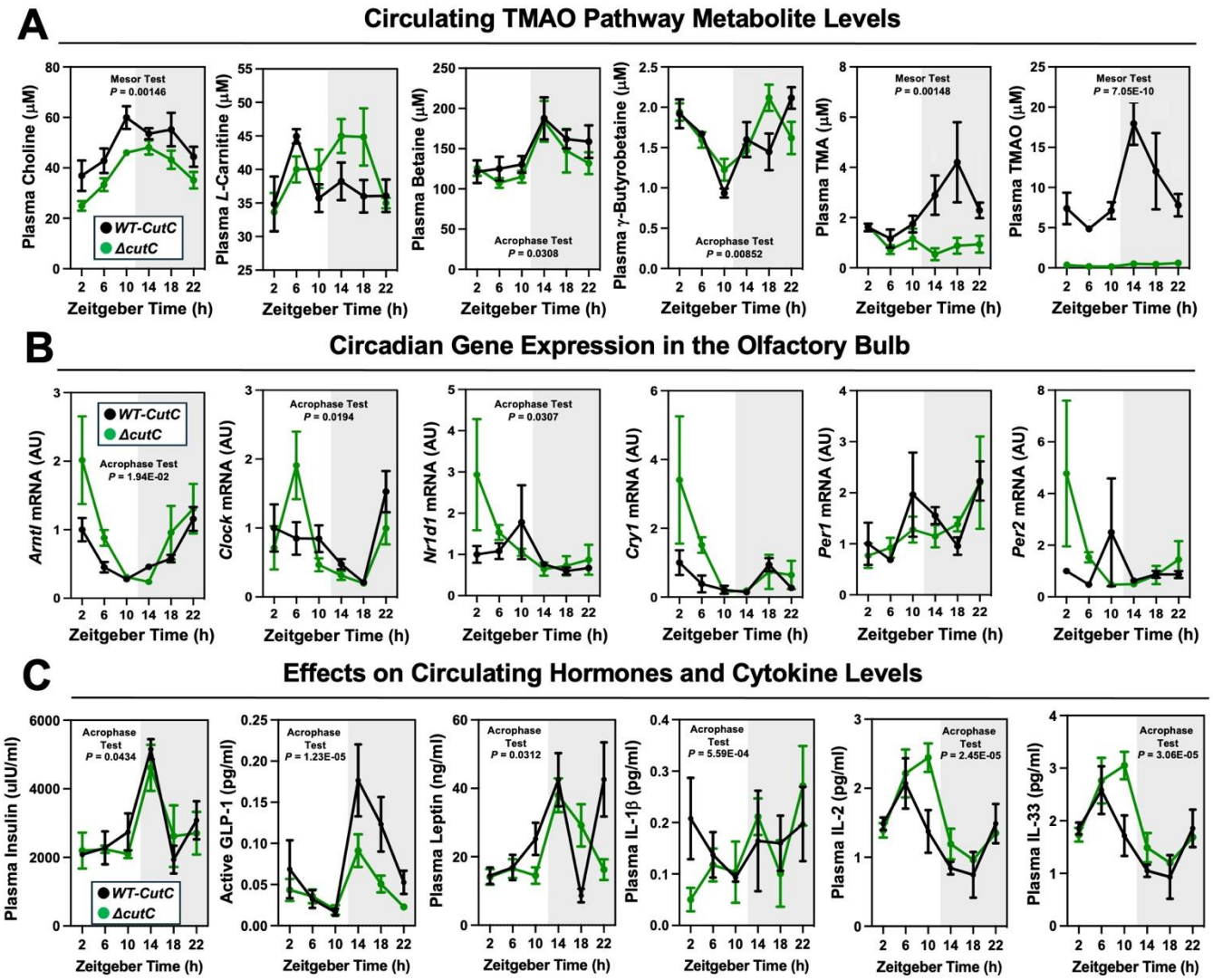

Figure 4 – figure supplement 1

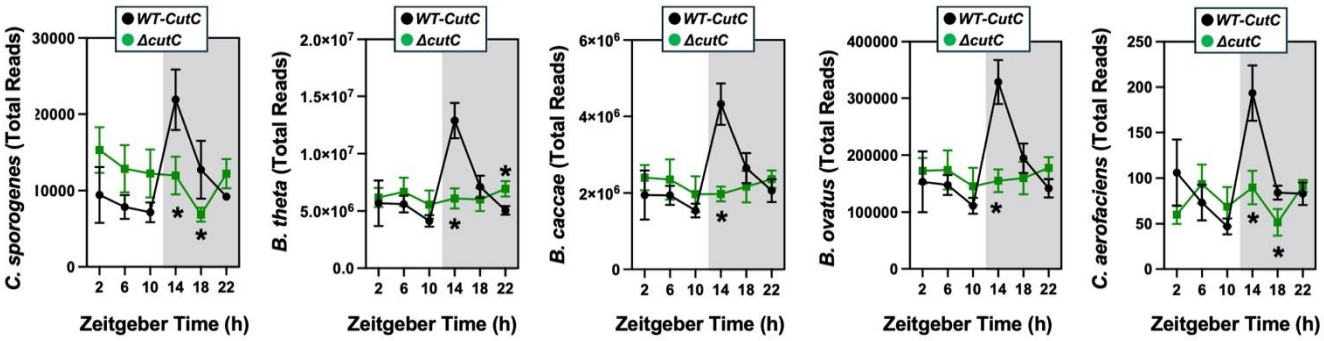

Figure 4 – figure supplement 2

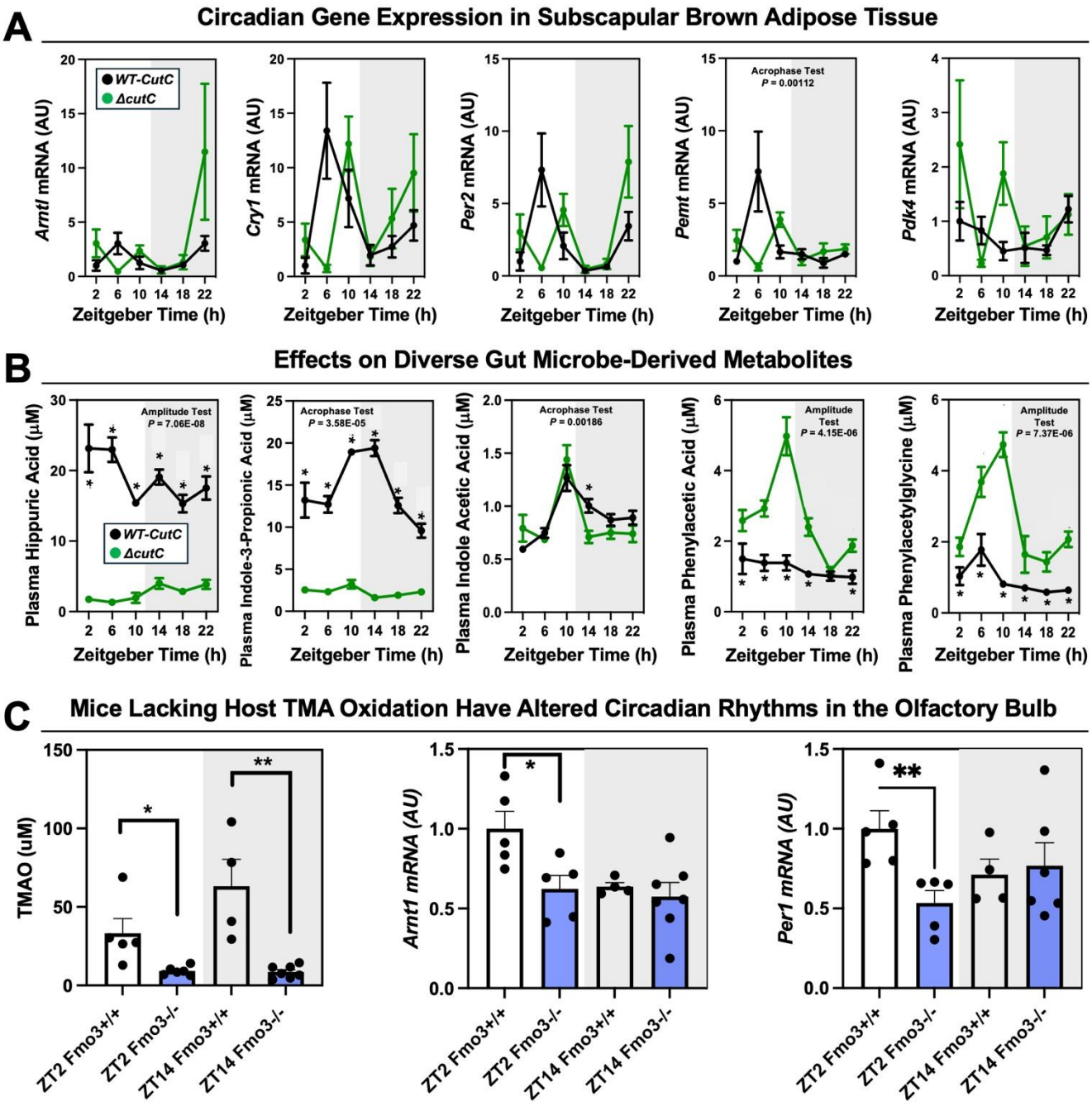

Table 1. Cosinor statistics for all circadian data include in this manuscript.

	Gene	Group	Zero Amplitude Test	MESOR	Amplitude	Acrophase	Mesor Test	Amplitude Test	Acrophase Comparison
Figure 1A: Skeletal Muscle Gene Expression	*LacZ*	Taar5 +/+	**1.82E-02**	4.754 ± 24.113	9.899 ± 33.683	14.295 ± 6.688			
		Taar5-/-	1.19E-01	141.511 ± 34.834	251.811 ± 35.373	19.3 ± 0.327	**2.85E-04**	**1.82E-02**	2.58E-01
	Arntl	Taar5 +/+	6.53E-02	0.555 ± 0.062	0.796 ± 0.086	3.132 ± 0.368			
		Taar5-/-	**2.84E-02**	0.497 ± 0.089	0.735 ± 0.098	3.747 ± 0.36	2.58E-01	8.30E-01	1.61E-01
	Nr1d1	Taar5 +/+	**1.24E-07**	0.553 ± 0.048	1.072 ± 0.066	4.301 ± 0.132			
		Taar5-/-	**6.09E-05**	0.521 ± 0.069	0.961 ± 0.074	5.52 ± 0.153	3.79E-01	6.28E-01	**2.76E-03**
	Per1	Taar5 +/+	**6.67E-05**	4.129 ± 0.987	7.785 ± 1.37	15.644 ± 0.388			
		Taar5-/-	5.31E-02	5.215 ± 1.426	10.66 ± 1.547	15.13 ± 0.252	3.38E-01	6.53E-01	2.10E-01
	Per2	Taar5 +/+	**1.45E-04**	2.679 ± 0.198	4.415 ± 0.278	13.325 ± 0.161			
		Taar5-/-	**2.26E-07**	2.708 ± 0.286	4.364 ± 0.285	12.193 ± 0.182	9.94E-01	6.54E-01	1.03E-01
Figure 1B: Olfactory Bulb Gene Expression	*Arntl*	Taar5 +/+	1.26E-01	1.167 ± 0.086	1.408 ± 0.117	16.412 ± 0.526			
		Taar5-/-	**1.12E-02**	1.523 ± 0.127	2.027 ± 0.142	5.045 ± 0.249	**2.44E-03**	6.28E-01	8.57E-02
	Clock	Taar5 +/+	**2.71E-02**	1.332 ± 0.162	2.065 ± 0.226	15.18 ± 0.318			
		Taar5-/-	5.56E-01	1.883 ± 0.243	2.134 ± 0.274	16.571 ± 0.955	**9.77E-03**	3.13E-01	**1.92E-02**
	Nr1d1	Taar5 +/+	**1.23E-04**	0.556 ± 0.052	0.93 ± 0.072	3.843 ± 0.198			
		Taar5-/-	**3.46E-02**	0.755 ± 0.077	0.984 ± 0.08	19.443 ± 0.364	**1.74E-02**	7.88E-01	**5.11E-04**
	Cry1	Taar5 +/+	9.27E-01	1.372 ± 0.108	1.443 ± 0.15	3.94 ± 2.197			
		Taar5-/-	**1.00E-03**	1.104 ± 0.162	1.575 ± 0.162	23.233 ± 0.385	1.61E-01	5.40E-01	**1.51E-02**
	Per2	Taar5 +/+	**4.14E-02**	0.829 ± 0.072	1.16 ± 0.1	5.245 ± 0.31			
		Taar5-/-	**2.17E-02**	0.498 ± 0.107	0.697 ± 0.106	21.328 ± 0.61	**3.05E-02**	6.25E-01	**7.66E-03**
Figure 1C: Liver Gene Expression	*Arntl*	Taar5 +/+	**5.81E-03**	0.519 ± 0.076	0.936 ± 0.102	0.695 ± 0.273			
		Taar5-/-	**2.56E-03**	0.614 ± 0.112	1.006 ± 0.113	23.712 ± 0.304	9.84E-01	6.46E-01	6.64E-02
	Cry1	Taar5 +/+	**1.15E-02**	0.471 ± 0.099	0.951 ± 0.132	0.7 ± 0.309			
		Taar5-/-	**2.06E-02**	0.552 ± 0.143	0.945 ± 0.141	23.773 ± 0.391	9.67E-01	6.30E-01	1.19E-01
	Cry2	Taar5 +/+	3.52E-01	0.877 ± 0.248	1.504 ± 0.351	3.887 ± 0.56			
		Taar5-/-	4.72E-01	0.88 ± 0.363	1.186 ± 0.361	23.798 ± 1.283	7.41E-01	4.80E-01	1.54E-01
	Per1	Taar5 +/+	**3.82E-03**	0.669 ± 0.051	0.909 ± 0.069	1.936 ± 0.313			
		Taar5-/-	3.24E-01	0.862 ± 0.074	0.999 ± 0.08	2.983 ± 0.541	1.23E-01	5.31E-01	7.81E-02
	Per2	Taar5 +/+	**2.80E-02**	0.602 ± 0.086	0.979 ± 0.116	0.775 ± 0.344			
		Taar5-/-	**1.20E-02**	0.594 ± 0.125	0.947 ± 0.121	23.21 ± 0.386	6.76E-01	6.12E-01	1.54E-01
Figure 1D: Gonadal White Adipose Tissue Gene Expression	*Arntl*	Taar5 +/+	5.01E-02	0.957 ± 0.052	1.114 ± 0.076	22.091 ± 0.46			
		Taar5-/-	**2.70E-04**	1 ± 0.078	1.468 ± 0.074	23.151 ± 0.197	7.46E-01	**2.13E-02**	**2.14E-02**
	Per1	Taar5 +/+	**1.53E-03**	2.093 ± 0.241	3.37 ± 0.35	11.239 ± 0.258			
		Taar5-/-	9.96E-01	2.825 ± 0.358	2.857 ± 0.331	9.766 ± 13.132	1.28E-01	8.66E-01	6.56E-02
	Per2	Taar5 +/+	**5.72E-05**	3.044 ± 0.433	5.964 ± 0.629	11.171 ± 0.203			
		Taar5-/-	3.74E-01	3.164 ± 0.642	4.201 ± 0.612	11.167 ± 0.732	4.39E-01	9.09E-01	**3.32E-02**
	Prdm16	Taar5 +/+	7.83E-01	1.388 ± 0.321	1.609 ± 0.46	21.199 ± 2.018			
		Taar5-/-	1.25E-01	2.842 ± 0.476	4.218 ± 0.509	19.065 ± 0.373	**2.42E-02**	3.88E-01	**6.89E-03**
	Ucp1	Taar5 +/+	6.30E-02	0.822 ± 0.048	1.003 ± 0.066	4.067 ± 0.385			
		Taar5-/-	7.15E-02	0.733 ± 0.072	0.908 ± 0.082	2.154 ± 0.404	1.15E-01	9.64E-01	3.39E-01

Figure 1: FS1: Body Weight	**Body Weight (g)**	Taar5 +/+	7.68E-01	27.721 ± 0.439	28.28 ± 0.619	23.314 ± 1.114			
		Taar5-/-	9.76E-01	28.602 ± 0.65	28.694 ± 0.709	2.096 ± 7.14	1.91E-01	6.85E-01	4.76E-01
Figure 1: FS2A: Circulating Metabolites	**Plasma Choline**	Taar5 +/+	**4.90E-02**	36.34 ± 1.937	43.346 ± 2.69	15.649 ± 0.397			
		Taar5-/-	1.25E-01	39.974 ± 2.855	47.106 ± 3.279	16.001 ± 0.383	3.63E-01	9.33E-01	1.28E-01
	Plasma L-Carnitine	Taar5 +/+	8.53E-01	24.784 ± 0.781	25.398 ± 1.085	13.785 ± 1.832			
		Taar5-/-	8.06E-01	26.771 ± 1.17	27.576 ± 1.242	13.292 ± 1.563	9.77E-02	7.70E-01	5.40E-01
	Plasma γ-Butyrobetaine	Taar5 +/+	5.02E-01	0.49 ± 0.029	0.53 ± 0.04	15.429 ± 1.027			
		Taar5-/-	9.76E-01	0.528 ± 0.043	0.539 ± 0.045	7.077 ± 4.027	6.30E-01	7.86E-01	**6.70E-07**
	Plasma TMA	Taar5 +/+	5.33E-02	43.982 ± 3.752	54.949 ± 5.213	16.683 ± 0.491			
		Taar5-/-	**4.73E-02**	48.983 ± 5.53	67.433 ± 5.893	18.815 ± 0.314	4.46E-01	5.55E-01	1.11E-01
	Plasma TMAO	Taar5 +/+	8.26E-01	4.139 ± 0.293	4.409 ± 0.41	14.115 ± 1.549			
		Taar5-/-	2.19E-01	4.124 ± 0.446	4.88 ± 0.454	21.652 ± 0.657	9.24E-01	6.91E-01	3.46E-01
Figure 1: FS2B: Circulating Hormones & Cytokines	**Plasma Insulin**	Taar5 +/+	6.30E-01	247.888 ± 17.712	272.029 ± 24.564	1.842 ± 1.057			
		Taar5-/-	1.97E-01	276.739 ± 26.221	331.367 ± 29.375	16.634 ± 0.47	2.86E-01	7.20E-01	2.67E-01
	Plasma C-Peptide	Taar5 +/+	7.10E-01	22.174 ± 11.509	36.075 ± 16.111	0.055 ± 1.183			
		Taar5-/-	4.78E-01	14.894 ± 17.249	36.615 ± 18.463	18.571 ± 0.831	6.32E-01	9.96E-01	4.47E-01
	Plasma Glucagon	Taar5 +/+	5.53E-02	17.512 ± 2.422	23.735 ± 3.481	9.044 ± 0.541			
		Taar5-/-	**4.32E-02**	20.612 ± 3.585	32.869 ± 3.499	10.213 ± 0.329	8.05E-02	2.59E-01	**3.27E-02**
	Plasma Active GLP-1	Taar5 +/+	3.40E-01	0.119 ± 0.015	0.157 ± 0.022	8.987 ± 0.56			
		Taar5-/-	2.40E-01	0.1 ± 0.022	0.135 ± 0.025	4.915 ± 0.642	5.27E-01	8.90E-01	**2.74E-05**
	Plasma Leptin	Taar5 +/+	9.39E-01	3758.578 ± 368.525	3912.379 ± 520.425	23.143 ± 3.393			
		Taar5-/-	5.79E-01	4704.115 ± 545.559	5435.666 ± 593.184	13.953 ± 0.758	**3.79E-02**	7.31E-01	5.29E-01
	Plasma Ghrelin	Taar5 +/+	**3.87E-02**	4.127 ± 2.019	10.62 ± 2.855	10.977 ± 0.44			
		Taar5-/-	6.43E-01	3.689 ± 3.025	7.185 ± 3.102	23.721 ± 0.944	9.26E-01	6.46E-01	2.13E-01
	Plasma PYY	Taar5 +/+	5.41E-01	99.806 ± 6.392	111.17 ± 9.13	6.039 ± 0.788			
		Taar5-/-	3.43E-01	87.449 ± 9.463	99.271 ± 9.243	21.654 ± 0.899	4.42E-01	7.12E-01	3.29E-01
	Plasma MCP-1	Taar5 +/+	**3.48E-02**	17.669 ± 3.13	28.406 ± 4.473	21.887 ± 0.408			
		Taar5-/-	**9.20E-03**	24.668 ± 4.633	43.882 ± 4.805	0.609 ± 0.257	3.39E-01	6.61E-01	**1.03E-02**
	Plasma IL-6	Taar5 +/+	**3.72E-02**	14.572 ± 4.767	30.045 ± 6.839	21.367 ± 0.429			
		Taar5-/-	**1.99E-02**	22.187 ± 7.057	49.695 ± 7.476	1.179 ± 0.268	4.48E-01	6.88E-01	8.54E-02
	Plasma TNFα	Taar5 +/+	**3.32E-02**	4.554 ± 0.25	5.526 ± 0.349	3.684 ± 0.368			
		Taar5-/-	**4.59E-03**	4.898 ± 0.37	6.47 ± 0.405	2.231 ± 0.237	2.43E-01	4.84E-01	**3.88E-02**

Figure 3: FS1: Gut-Microbial Oscillations	*Lachnospiraceae UCG-002*	Taar5 +/+	5.97E-01	0.006 ± 0.002	0.008 ± 0.002	17.331 ± 1.392			
		Taar5-/-	8.35E-02	0.008 ± 0.002	0.015 ± 0.002	23.636 ± 0.37	8.17E-01	6.95E-01	**7.67E-15**
	Lachnospiraceae UCG-006	Taar5 +/+	**1.37E-02**	0.002 ± 0	0.004 ± 0.001	18.976 ± 0.324			
		Taar5-/-	6.36E-01	0.002 ± 0.001	0.002 ± 0.001	17.578 ± 0.899	9.84E-01	5.01E-01	**5.83E-14**
	Lachnospiraceae NK4A136	Taar5 +/+	3.30E-01	0.151 ± 0.013	0.18 ± 0.018	17.153 ± 0.656			
		Taar5-/-	**1.13E-02**	0.177 ± 0.019	0.237 ± 0.019	20.216 ± 0.349	4.09E-01	5.61E-01	**2.43E-05**
	Lactobacillus	Taar5 +/+	**4.33E-02**	0.047 ± 0.005	0.065 ± 0.007	5.41 ± 0.414			
		Taar5-/-	5.95E-01	0.042 ± 0.008	0.052 ± 0.009	4.807 ± 0.803	1.53E-01	8.31E-01	5.14E-01
	Desulfovibrio	Taar5 +/+	3.62E-01	0.017 ± 0.001	0.02 ± 0.002	5.011 ± 0.629			
		Taar5-/-	2.06E-01	0.02 ± 0.002	0.022 ± 0.002	8.832 ± 0.802	2.25E-01	9.14E-01	**8.89E-13**
	Bacteroides	Taar5 +/+	1.27E-01	0.003 ± 0.001	0.005 ± 0.001	12.204 ± 0.658			
		Taar5-/-	1.50E-01	0.005 ± 0.001	0.008 ± 0.001	17.39 ± 0.35	8.12E-02	3.38E-01	**1.80E-15**
	Dubosiella	Taar5 +/+	**1.75E-02**	0.024 ± 0.006	0.04 ± 0.008	3.971 ± 0.538			
		Taar5-/-	6.40E-01	0.043 ± 0.009	0.054 ± 0.009	20.383 ± 0.88	**3.71E-02**	3.41E-01	**1.09E-07**
	Faecalibaculum	Taar5 +/+	1.04E-01	0.435 ± 0.021	0.494 ± 0.029	5.808 ± 0.517			
		Taar5-/-	**2.03E-02**	0.374 ± 0.031	0.484 ± 0.032	7.548 ± 0.303	1.28E-01	4.70E-01	**4.97E-03**
	Colidextribacter	Taar5 +/+	2.04E-01	0.009 ± 0.001	0.01 ± 0.001	0.165 ± 0.725			
		Taar5-/-	1.78E-01	0.009 ± 0.001	0.011 ± 0.001	21.769 ± 0.47	5.77E-01	5.24E-01	**7.46E-16**
	Odoribacter	Taar5 +/+	3.48E-01	0.003 ± 0	0.004 ± 0.001	18.339 ± 0.939			
		Taar5-/-	2.71E-01	0.004 ± 0.001	0.005 ± 0.001	14.39 ± 0.436	3.29E-01	7.73E-01	**1.18E-13**
	Butyricicoccus	Taar5 +/+	5.02E-02	0.001 ± 0	0.002 ± 0	17.635 ± 0.403			
		Taar5-/-	8.12E-01	0.001 ± 0	0.002 ± 0	2.352 ± 1.401	5.94E-01	6.72E-01	**4.78E-16**
	Alistipes	Taar5 +/+	5.71E-01	0.012 ± 0.001	0.014 ± 0.001	17.299 ± 0.909			
		Taar5-/-	**1.21E-02**	0.015 ± 0.002	0.02 ± 0.002	17.706 ± 0.309	1.23E-01	3.38E-01	**1.30E-09**
	Turicibacter	Taar5 +/+	**4.53E-02**	0.02 ± 0.003	0.03 ± 0.004	12.019 ± 0.382			
		Taar5-/-	3.36E-01	0.025 ± 0.004	0.032 ± 0.004	13.386 ± 0.609	1.57E-01	7.19E-01	**7.79E-10**
	Muribaculum	Taar5 +/+	**5.26E-03**	0.015 ± 0.001	0.019 ± 0.001	8.483 ± 0.3			
		Taar5-/-	6.65E-01	0.018 ± 0.001	0.019 ± 0.001	13.769 ± 0.91	**4.95E-02**	5.29E-01	**2.37E-14**
	Coriobacteriaceae UCG-002	Taar5 +/+	1.51E-01	0.001 ± 0	0.001 ± 0	17.27 ± 0.423			
		Taar5-/-	1.23E-01	0 ± 0	0.001 ± 0	9.186 ± 0.877	2.81E-01	6.11E-01	**1.45E-16**
	Acetatifactor	Taar5 +/+	3.19E-01	0 ± 0	0 ± 0	21.763 ± 0.938			
		Taar5-/-	**1.92E-02**	0.001 ± 0	0.002 ± 0	12.15 ± 0.259	**1.00E-02**	8.33E-02	**4.02E-17**
	A2	Taar5 +/+	6.79E-01	0.003 ± 0.001	0.004 ± 0.001	21.902 ± 1.096			
		Taar5-/-	5.48E-01	0.005 ± 0.001	0.006 ± 0.001	17.624 ± 0.794	5.63E-02	8.03E-01	**6.74E-10**
	Helicobacter	Taar5 +/+	**3.17E-02**	0.108 ± 0.009	0.144 ± 0.012	19.101 ± 0.34			
		Taar5-/-	1.41E-01	0.117 ± 0.013	0.143 ± 0.013	20.176 ± 0.539	5.14E-01	9.05E-01	**5.81E-06**
	Parabacteroides	Taar5 +/+	5.90E-02	0.005 ± 0.001	0.007 ± 0.001	18.585 ± 0.551			
		Taar5-/-	2.64E-01	0.005 ± 0.001	0.008 ± 0.001	23.917 ± 0.491	5.54E-01	4.22E-01	**1.18E-15**
	Anaerotruncus	Taar5 +/+	8.75E-01	0.001 ± 0	0.001 ± 0	20.55 ± 1.74			
		Taar5-/-	**2.18E-02**	0.001 ± 0	0.002 ± 0	16.818 ± 0.302	8.81E-01	4.83E-01	**2.76E-18**

Figure 4A: Circulating Metabolites	**Plasma Choline**	WT-CutC	**5.24E-03**	48.996 ± 1.613	59.468 ± 2.293	13.545 ± 0.217			
		ΔCutC	**4.47E-07**	38.449 ± 2.182	49.649 ± 2.079	13.901 ± 0.186	**1.46E-03**	7.74E-01	**9.62E-03**
	Plasma L-Carnitine	WT-CutC	3.97E-01	37.502 ± 1.209	39.803 ± 1.709	7.059 ± 0.743			
		ΔCutC	**7.91E-03**	39.771 ± 1.636	45.211 ± 1.558	13.95 ± 0.286	3.91E-01	3.99E-01	7.81E-02
	Plasma Betaine	WT-CutC	**1.79E-02**	147.098 ± 7.387	177.373 ± 10.633	16.69 ± 0.339			
		ΔCutC	**3.16E-02**	135.295 ± 9.995	163.756 ± 9.522	16.348 ± 0.335	2.36E-01	9.60E-01	**3.08E-02**
	Plasma γ-Butyrobetaine	WT-CutC	**8.38E-04**	1.605 ± 0.073	2.062 ± 0.102	23.336 ± 0.229			
		ΔCutC	**1.28E-02**	1.66 ± 0.099	1.959 ± 0.094	21.842 ± 0.314	6.75E-01	4.08E-01	**8.52E-03**
	Plasma TMA	WT-CutC	**1.41E-02**	2.315 ± 0.217	3.654 ± 0.312	17.405 ± 0.226			
		ΔCutC	2.03E-01	0.984 ± 0.294	1.298 ± 0.28	2.228 ± 0.894	**1.48E-03**	3.21E-01	**7.76E-03**
	Plasma TMAO	WT-CutC	**8.91E-03**	9.425 ± 0.694	14.543 ± 1	15.901 ± 0.188			
		ΔCutC	**3.78E-03**	0.378 ± 0.939	0.584 ± 0.894	19.563 ± 4.339	**7.05E-10**	9.04E-02	**1.66E-05**
Figure 4B: Olfactory Bulb Gene Expression	*Arntl*	WT-CutC	**1.29E-05**	0.655 ± 0.12	1.076 ± 0.169	23.101 ± 0.401			
		ΔCutC	**1.29E-03**	0.951 ± 0.16	1.759 ± 0.151	0.492 ± 0.187	1.28E-01	5.48E-01	**1.94E-02**
	Clock	WT-CutC	5.92E-02	0.827 ± 0.124	1.214 ± 0.177	2.015 ± 0.447			
		ΔCutC	**6.50E-03**	0.766 ± 0.167	1.377 ± 0.159	4.265 ± 0.261	6.89E-01	6.55E-01	**3.07E-02**
	Nr1d1	WT-CutC	1.90E-01	0.998 ± 0.232	1.484 ± 0.325	8.312 ± 0.684			
		ΔCutC	**4.22E-02**	1.294 ± 0.315	2.208 ± 0.3	3.218 ± 0.328	4.61E-01	6.35E-01	1.64E-01
	Cry1	WT-CutC	1.57E-01	0.49 ± 0.28	0.761 ± 0.391	23.237 ± 1.484			
		ΔCutC	**3.82E-02**	1.105 ± 0.38	2.393 ± 0.362	2.249 ± 0.281	1.52E-01	5.21E-01	1.70E-01
	Per1	WT-CutC	7.50E-01	1.42 ± 0.203	1.657 ± 0.292	15.948 ± 1.188			
		ΔCutC	2.86E-01	1.283 ± 0.274	1.684 ± 0.261	19.535 ± 0.652	4.31E-01	7.79E-01	2.27E-01
	Per2	WT-CutC	7.06E-01	1.095 ± 0.49	1.588 ± 0.679	10.038 ± 1.435			
		ΔCutC	6.56E-02	1.594 ± 0.663	3.301 ± 0.632	1.821 ± 0.37	5.52E-01	4.24E-01	1.65E-01
Figure 4C: Circulating Hormones & Cytokines	**Plasma Insulin**	WT-CutC	6.53E-02	2855.806 ± 256.148	3745.034 ± 366.205	14.161 ± 0.403			
		ΔCutC	6.02E-02	2771.925 ± 349.484	3634.451 ± 337.861	15.525 ± 0.388	9.83E-01	8.89E-01	**4.34E-02**
	Plasma Active GLP-1	WT-CutC	**1.55E-02**	0.076 ± 0.01	0.135 ± 0.014	16.858 ± 0.234			
		ΔCutC	1.00E-01	0.044 ± 0.014	0.063 ± 0.013	15.187 ± 0.685	**9.63E-04**	4.56E-01	**1.23E-05**
	Plasma Leptin	WT-CutC	5.34E-01	25.035 ± 2.737	30.766 ± 3.944	15.842 ± 0.662			
		ΔCutC	**8.20E-04**	21.468 ± 3.734	32.134 ± 3.61	15.542 ± 0.335	5.30E-01	4.47E-01	**3.12E-02**
	Plasma IL-1β	WT-CutC	5.63E-01	0.162 ± 0.027	0.205 ± 0.038	22.624 ± 0.88			
		ΔCutC	1.95E-01	0.145 ± 0.037	0.217 ± 0.039	17.696 ± 0.464	6.50E-01	8.98E-01	**5.59E-04**
	Plasma IL-2	WT-CutC	**4.21E-03**	1.342 ± 0.102	1.936 ± 0.141	4.542 ± 0.25			
		ΔCutC	**5.82E-04**	1.562 ± 0.145	2.245 ± 0.152	7.478 ± 0.202	9.45E-02	8.14E-01	**2.45E-05**
	Plasma IL-33	WT-CutC	**4.21E-03**	1.675 ± 0.128	2.417 ± 0.176	4.542 ± 0.25			
		ΔCutC	**5.82E-04**	1.95 ± 0.181	2.802 ± 0.19	7.478 ± 0.202	9.45E-02	8.14E-01	**3.06E-05**

Figure 4: FS1: Gut-Microbial Oscillations	*C. sporogenes*	WT-CutC	**4.26E-02**	11207.569 ± 1203.539	16210.557 ± 1734.346	15.823 ± 0.334			
		ΔCutC	1.91E-01	11870.76 ± 1642.087	14613.721 ± 1553.3	4.704 ± 0.585	7.45E-01	6.15E-01	9.93E-02
	B. theta	WT-CutC	**4.02E-02**	6627371.809 ± 539206.187	9170588.869 ± 776361.623	15.395 ± 0.294			
		ΔCutC	7.77E-01	6231828.204 ± 735683.26	6635937.065 ± 713176.544	0.156 ± 1.738	3.76E-01	3.76E-01	1.85E-01
	B. caccae	WT-CutC	**2.52E-02**	2376257.403 ± 184646.029	3267446.417 ± 266090.328	15.862 ± 0.287			
		ΔCutC	5.14E-01	2206196.864 ± 251927.734	2453122.904 ± 242269.927	1.047 ± 0.982	3.23E-01	4.42E-01	1.64E-01
	B. ovatus	WT-CutC	**4.01E-02**	176638.846 ± 13904.713	241069.256 ± 20033.622	15.68 ± 0.299			
		ΔCutC	6.37E-01	164003.694 ± 18971.341	178418.111 ± 18317.846	0.612 ± 1.262	3.31E-01	4.21E-01	1.87E-01
	C. aerofaciens	WT-CutC	2.79E-01	95.96 ± 9.973	124.552 ± 14.366	16.401 ± 0.484			
		ΔCutC	8.03E-01	75.142 ± 13.607	81.998 ± 13.201	7.939 ± 1.893	1.67E-01	4.80E-01	1.22E-01
Figure 4: FS2A: Brown Adipose Tissue Gene Expression	*Arntl*	WT-CutC	1.80E-01	1.653 ± 0.958	2.44 ± 1.37	2.207 ± 1.703			
		ΔCutC	1.03E-01	3.207 ± 1.296	6.833 ± 1.235	22.489 ± 0.341	2.39E-01	3.26E-01	1.76E-01
	Crgl	WT-CutC	6.33E-02	5.132 ± 1.197	9.024 ± 1.694	6.937 ± 0.435			
		ΔCutC	8.66E-01	5.491 ± 1.62	6.374 ± 1.543	16.558 ± 1.749	9.10E-01	3.75E-01	1.32E-01
	Pet2	WT-CutC	5.80E-02	2.436 ± 0.668	4.608 ± 0.962	4.858 ± 0.428			
		ΔCutC	2.02E-01	2.885 ± 0.904	4.606 ± 0.862	23.517 ± 0.5	6.70E-01	7.99E-01	8.42E-02
	Pemt	WT-CutC	6.35E-02	2.222 ± 0.436	4.201 ± 0.622	6.133 ± 0.309			
		ΔCutC	7.58E-01	1.925 ± 0.595	2.225 ± 0.581	8.928 ± 1.881	4.09E-01	2.46E-01	**1.12E-03**
	Pdk4	WT-CutC	**3.82E-02**	0.747 ± 0.227	1.118 ± 0.321	0.763 ± 0.867			
		ΔCutC	5.39E-01	1.156 ± 0.31	1.587 ± 0.294	2.611 ± 0.701	2.83E-01	9.45E-01	3.94E-01
Figure 4: FS2B: Gut Microbe-Derived Metabolites	**Plasma Hippuric Acid**	WT-CutC	**2.81E-02**	18.787 ± 0.579	22.187 ± 0.834	3.601 ± 0.236			
		ΔCutC	**6.06E-03**	2.619 ± 0.784	3.83 ± 0.747	17.698 ± 0.617	**7.06E-08**	2.82E-01	1.07E-01
	lasma Indole-3-Propionic Ac	WT-CutC	**1.79E-05**	14.418 ± 0.371	18.964 ± 0.518	11.514 ± 0.117			
		ΔCutC	6.44E-02	2.319 ± 0.503	2.757 ± 0.479	5.969 ± 1.093	**1.19E-08**	**1.10E-03**	**3.58E-05**
	Plasma Indole Acetic Acid	WT-CutC	**1.48E-03**	0.903 ± 0.052	1.145 ± 0.073	12.622 ± 0.306			
		ΔCutC	**3.94E-02**	0.853 ± 0.071	1.062 ± 0.067	9.908 ± 0.322	2.08E-01	9.01E-01	**1.86E-03**
	Plasma Phenylacetic Acid	WT-CutC	1.51E-01	1.224 ± 0.149	1.49 ± 0.213	5.923 ± 0.783			
		ΔCutC	**1.06E-05**	2.654 ± 0.202	4.068 ± 0.192	8.438 ± 0.136	**4.15E-06**	**2.35E-02**	**4.05E-03**
	Plasma Phenylacetylglycine	WT-CutC	**6.27E-03**	0.913 ± 0.166	1.388 ± 0.238	5.47 ± 0.488			
		ΔCutC	**6.54E-05**	2.573 ± 0.225	3.992 ± 0.214	7.993 ± 0.151	**7.37E-06**	1.82E-01	**6.91E-05**
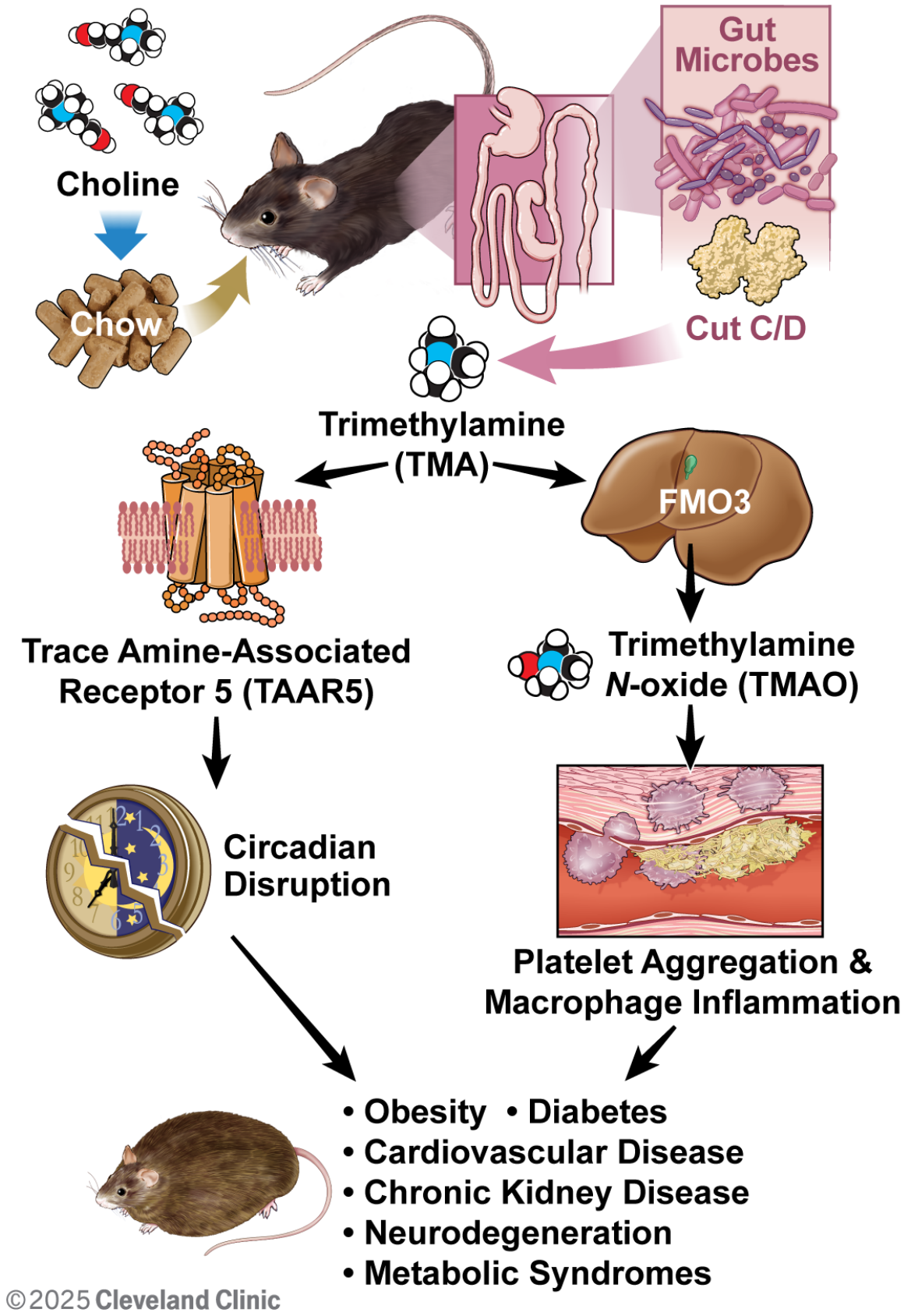
Graphical Abstract